Extensive H_2O degassing in deeply erupted submarine glasses inferred from Samoan melt inclusions: The EM2 mantle source is damp, not dry

O. E. Anderson[1*], M. G. Jackson[1], A. S. Pamukçu[2,3], E. F. Rose-Koga[4], V. Le Roux[2], F. Klein[2], K. T. Koga[4], G. A. Gaetani[2], A. A. Price[1]

[1]Isotope Geochemistry Facility – Global Center for Mantle Zoology (GCMZ), University of California Santa Barbara, Department of Earth Science, Santa Barbara, CA, USA [2]Woods Hole Oceanographic Institution, Woods Hole, Massachusetts 02543, USA [3]Geological Sciences, Stanford University, Stanford, CA, USA [4]Institut des Sciences de la Terre d'Orléans (ISTO), UO/CNRS/BRGM, 1A rue de la Férollerie, 45071, Orléans, France

*Corresponding author: Olivia E. Anderson (anderson03@ucsb.edu)

Highlights:

- Samoan melt inclusions have higher H_2O/Ce—indicating less degassing—compared to Samoan pillow glasses.
- High $^{87}Sr/^{86}Sr$ melt inclusions have high H_2O/Ce, contrary to prior observations using pillow glasses.
- Low H_2O/Ce in high $^{87}Sr/^{86}Sr$ glasses indicates extensive degassing has occurred, so cannot be used to infer mantle H_2O/Ce.
- Melt inclusions show that enriched mantle (EM) lavas have H_2O/Ce similar to non-EM lavas.
- Elevated CO_2 in EM melts leads to greater degassing and lower H_2O/Ce in erupted glasses compared to depleted mantle.

Find the final version of the article at:

Anderson, O.E., Jackson, M.G., Pamukçu, A.S., Rose-Koga, E.F., Le Roux, V., Klein, F., Koga, K.T., Gaetani, G.A. and Price, A.A. (2024). Extensive H_2O degassing in deeply erupted submarine glasses inferred from Samoan melt inclusions: The EM2 mantle source is damp, not dry. *Chemical Geology*, 651, 121979. https://doi.org/10.1016/j.chemgeo.2024.121979

Abstract

Submarine glasses erupted at intraplate volcanic hotspot settings sampling enriched mantle (EM)—characterized by high $^{87}Sr/^{86}Sr$—exhibit lower H_2O/Ce than glasses representing less enriched mantle domains, leading to the interpretation that the EM mantle is H_2O-poor ("dry"). We test whether low H_2O/Ce observed in pillow glasses of EM lavas resulted from degassing of higher H_2O/Ce primary melts by measuring H_2O/Ce and $^{87}Sr/^{86}Sr$ in olivine-hosted melt inclusions from two deeply-erupted (3950 and 2190 meters below sea level (mbsl)) Samoan submarine lavas from Vailulu'u and Malumalu seamounts. Vailulu'u (H_2O/Ce=161–275) and Malumalu (149–232) melt inclusions have an average H_2O/Ce (197±58 2SD, N=15) that is nearly twice as high as H_2O/Ce in pillow glasses from these two seamounts (average H_2O/Ce=106±51, N=65). Notably, the average H_2O/Ce of Samoan melt inclusions (197±58) is comparable to pillow glasses from non-EM hotspots. We show that lower H_2O/Ce in submarine Samoan glasses compared to melt inclusions results from greater closed-system degassing, and concomitant loss of H_2O, because EM melts have higher initial concentrations of CO_2. We show that the lower H_2O/Ce in global EM pillow glasses compared to non-EM pillow glasses can be modeled to be the result of more extensive degassing of H_2O in EM melts, which owes to higher CO_2 in primary melts (20,000–90,000 ppm) of EM sources compared to non-EM melts (300–50,000 ppm CO_2). Instead of originating from a dry mantle, we conclude that EM lavas derive from a damp mantle, but EM melts lose more H_2O by degassing than non-EM melts.

Keywords: melt inclusion, Samoa, hotspot, degassing, enriched mantle, H_2O

1. Introduction

Although volatiles are a minor component in silicate melts, they play an outsize role on the properties and behavior of magmatic systems. Hydrogen and carbon affect the rheology of the mantle, the depth and extent of melting, the composition of melts, and how melts evolve (e.g., Asimow & Langmuir, 2003; Gaetani & Grove, 1998; Hirschmann, 2006; Hirth & Kohlstedt, 1996, 2003; Portnyagin et al., 2007). Therefore, connecting volatile element compositions to mantle domains characterized by particular isotopic compositions, such as enriched mantle (EM), can provide additional insights into mantle heterogeneities. A variety of geochemical "flavors" have been identified in the mantle via geochemical taxonomy of ocean island basalts (OIB), and the various mantle species are broadly encompassed by several canonical mantle endmembers that include HIMU (high $\mu=^{238}U/^{204}Pb$), EM1 (enriched mantle 1), EM2 (enriched mantle 2), and DM (depleted mantle). Samoan lavas have unique geochemical signatures that extend to Enriched Mantle 2 (EM2) isotopic compositions (e.g., high $^{87}Sr/^{86}Sr$, intermediate $^{206}Pb/^{204}Pb$, and low $^{143}Nd/^{144}Nd$). The EM2 mantle source has been suggested to be derived from recycled continental materials (e.g., White & Hofmann, 1982; White & Duncan, 1996; Jackson & Macdonald, 2022). Therefore, characterization of Samoan EM2 lavas can provide insights into the role that deep continental crust subduction plays in controlling the volatile budgets of the mantle.

The ratios H_2O/La or H_2O/Ce measured in submarine glasses are commonly used to evaluate H_2O enrichment or depletion in the mantle because H_2O, La, and Ce have similar degrees of incompatibility (e.g., Michael, 1995). Thus, their ratios are not significantly affected by partial melting and crystal fractionation. The EM2 mantle source has been interpreted to be 'dry' because the H_2O/Ce (or H_2O/La) is lower at higher $^{87}Sr/^{86}Sr$ for Samoan glasses (Workman

et al., 2006). Workman et al. (2006) found that H_2O/La anticorrelates with $^{87}Sr/^{86}Sr$: the more geochemically enriched (higher $^{87}Sr/^{86}Sr$) Samoan glasses have lower H_2O/La than more geochemically depleted Samoan glasses; the high H_2O/La MORB mantle endmember anchors the low $^{87}Sr/^{86}Sr$ portion of the array. Workman et al. (2006) explained this relationship between $^{87}Sr/^{86}Sr$ and H_2O/La as the result of diffusive H_2O loss from EM2 reservoirs during long-term storage in a dry and depleted mantle, resulting in a "dry" EM2 mantle domain that has low H_2O/La and low H_2O. Similarly, Dixon et al. (2002) found that high $^{87}Sr/^{86}Sr$ basalts erupted in MOR settings had low H_2O/Ce. However, unlike Workman et al. (2006), Dixon et al. (2002) suggested that the dry nature of the EM reservoir was due to dehydration of sediments during subduction, resulting in low H_2O/Ce signatures in subducted, dehydrated sediments, which ultimately contribute to enriched mantle domains. Bizimis and Peslier (2015) offered further discussion regarding the origin of apparently dry EM2 domains and argued that the low H_2O/Ce in EM lavas is the result of recycling of pyroxenite-bearing oceanic lithosphere. The pyroxenites they examined have low H_2O/Ce and high H_2O, a result of preferential partitioning of Ce into clinopyroxene compared to H_2O.

Additional work highlights the low H_2O/Ce in enriched mantle domains (Kendrick et al., 2017). In particular, classical EM1 and EM2 oceanic hotspots—Pitcairn and Societies, respectively—exhibit negative correlations between $^{87}Sr/^{86}Sr$ and H_2O/Ce in submarine glasses (Kendrick et al., 2014). Thus, low H_2O/Ce appears to be a defining feature of EM lavas, and constraining the origin of this geochemical signature is critical for understanding the origin of the EM mantle and/or the petrogenesis of EM lavas.

Existing models for the origin of low H_2O/La and H_2O/Ce in EM-flavored OIB pillow glasses quenched in deep submarine environments are predicated on the assumption that the low

H_2O/Ce is a source feature and the EM primary melts have low H_2O/Ce inherited from the mantle source (Dixon et al., 2002; Dixon & Clague, 2001; Wallace, 2002; Workman et al., 2006; Kendrick et al., 2014). This interpretation assumes that magmatic degassing follows open system behavior, a mechanism that results in significant loss of CO_2, but not H_2O, from the melt by degassing: the H_2O/Ce in deeply erupted glasses (i.e., ≥0.1 kbar; Workman et al., 2006) resulting from this process are similar to the mantle source despite having degassed most of their magmatic CO_2.

In this study, we test this assumption using combined H_2O/Ce and $^{87}Sr/^{86}Sr$ measurements in individual olivine-hosted melt inclusions isolated from two well-characterized submarine Samoan basalts that were characterized by Workman et al. (2006). We present volatile (H_2O, CO_2, Cl, F, S), major, and trace element concentrations and $^{87}Sr/^{86}Sr$ on Samoan melt inclusions from both samples—AVON3-78-1 and AVON3-71-2—which were obtained from Malumalu and Vailulu‘u seamounts, respectively. Malumalu lavas reach $^{87}Sr/^{86}Sr$ of up to 0.708901, which is the most extreme EM2 composition that we explore in this study. In contrast, Vailulu‘u lavas have $^{87}Sr/^{86}Sr$ that range from 0.705352 to 0.706720, and thus represent a less enriched composition at the Samoan hotspot. Previous $^{87}Sr/^{86}Sr$ analyses of Samoan melt inclusions demonstrated extreme heterogeneity (0.70434 to 0.70926) that has been verified using both *in situ* LA-ICP-MS approach (laser-ablation inductively coupled plasma mass spectrometry; Jackson & Hart, 2006) and an approach involving wet chemistry followed by TIMS (thermal ionization mass spectrometry; Reinhard et al., 2018). Critically for this study, the melt inclusions from the two lavas examined here span nearly the same range of $^{87}Sr/^{86}Sr$ (0.704858–0.709225) as identified in prior melt inclusion studies (Jackson & Hart, 2006; Reinhard et al., 2018) and have similar trace element characteristics as the Samoan glasses examined for H_2O/La and

131 $^{87}Sr/^{86}Sr$ by Workman et al. (2006) (0.704521–0.708901). We interpret this to indicate that the
132 melt inclusions thus sample the same mantle sources as the pillow glasses studied by Workman
133 et al. (2006).

134 However, Samoan melt inclusions in this study exhibit two key differences with the
135 Samoan submarine glasses reported in Workman et al. (2006): 1) the melt inclusions have higher
136 H_2O/Ce than Samoan submarine glasses and 2) the inclusions exhibit no relationship between
137 H_2O/Ce and $^{87}Sr/^{86}Sr$, which contrasts with the negative correlation between $^{87}Sr/^{86}Sr$ and
138 H_2O/Ce observed in Samoan pillow glasses. We model the difference in H_2O/Ce between melt
139 inclusions and pillow glasses as being a result of closed-system degassing, a mechanism that
140 results in greatly diminished CO_2 *and* H_2O concentrations in the melt (in contrast to open-system
141 degassing, which results in greatly diminished CO_2, but not H_2O, melt concentrations). In this
142 model, the melt inclusions experience less closed-system degassing compared to submarine
143 glasses because of deep entrapment of the melt inclusions in growing olivine crystals within
144 magma chambers. Melts that were not trapped continued to degas both CO_2 and H_2O up until
145 eruption and quenching on the seafloor, resulting in lower H_2O/Ce in the submarine glasses
146 compared to the deeply entrapped melt inclusions.

147 We also present a model suggesting that, across global oceanic hotspots, primary melts
148 with higher $^{87}Sr/^{86}Sr$ (e.g., Samoan and Societies EM2 glasses, Pitcairn EM1 glasses) have
149 higher primary melt CO_2 than lower $^{87}Sr/^{86}Sr$ melts (e.g., Foundation, Hawai‘i (Lō‘ihi), and
150 Easter hotspots). Higher CO_2 in high $^{87}Sr/^{86}Sr$ (EM) melts results in greater degassing of both
151 CO_2 and H_2O (and a greater reduction in the H_2O/Ce ratio) compared to low $^{87}Sr/^{86}Sr$ melts,
152 which explains the negative global correlation between H_2O/Ce and $^{87}Sr/^{86}Sr$ in OIB glasses.
153 This new result suggests that submarine glasses sourcing EM domains do not provide reliable

154 records for evaluating the H_2O and H_2O/Ce in the mantle source. In melt inclusions, degassing is
155 arrested at great depth, making it possible to identify H_2O/Ce ratios that are closer to values in
156 the primary melt.

157 **2. Methods**

158 Submarine pillow basalt samples in this study are from two Samoan seamounts (Figure 1)
159 that are young (<8 ka; Sims et al., 2008) and associated with visually fresh lavas: Malumalu
160 (sample AVON3-78-1; 2260–2190 mbsl) and Vailulu‘u (sample AVON3-71-2; 4420–3950
161 mbsl) are olivine-rich lavas with glassy chill margins on the pillow rims. Olivine-hosted melt
162 inclusions from Vailulu‘u and Malumalu seamounts in this study were rehomogenized on a
163 heating stage (see supplement for methods), and these rehomogenized inclusions were then
164 characterized for $^{87}Sr/^{86}Sr$ (15 melt inclusions total), $^{143}Nd/^{144}Nd$ (only three melt inclusions),
165 stable hydrogen isotope ratios (δD), and major, trace and volatile element concentrations (Table
166 S1). This supplement also includes methodological details for the glass major element (electron
167 microprobe), volatile (ion probe), hydrogen isotope (ion probe), and trace element (LA-ICP-MS)
168 analyses and the host olivine major element (electron microprobe) analyses. Strontium separation
169 chemistry and $^{87}Sr/^{86}Sr$ analyses by TIMS used in this study follow the same procedure as
170 described in Anderson et al. (2021). The supplement includes details of Nd separation chemistry
171 for melt inclusions, and $^{143}Nd/^{144}Nd$ analyses by TIMS at the University of California, Santa
172 Barbara Isotope Geochemistry Facility. Only three melt inclusions (all from the Vailulu‘u
173 Seamount sample) in this study had sufficient Nd for the isotopic analysis.

174 The results of *in situ* analyses (of δD, and major, trace and volatile element concentrations)
175 of geologic reference materials (ALV519-4-1, ALV1833-1, GL07 D52-5, and BCR-2) can be

found in Table S2, and $^{87}Sr/^{86}Sr$ and $^{143}Nd/^{144}Nd$ analyses of BCR-2 can be found in Tables S6 and S8.

Melt inclusion major, trace, and volatile element concentrations were corrected for post-entrapment crystallization (PEC) by addition or subtraction of equilibrium olivine in 0.1% increments until the major element composition of the inclusion is in equilibrium with the host olivine forsterite (Fo) content. In the calculation, two assumptions are made: (i) the olivine-melt Fe-Mg $K_d = 0.30$ (Roeder & Emslie, 1970; Ford et al., 1983; $K_d = (Fe^{2+}/Mg)_{olivine}/(Fe^{2+}/Mg)_{melt}$) and (ii) Fe^{3+} comprises 10% of the total moles of iron in the melt (following Hauri, 1996). Unless stated otherwise, all major, trace, and volatile element concentrations reported below have been corrected for equilibrium olivine addition/subtraction so that the inclusion is in equilibrium with the host olivine.

The supplement also details the method of accounting for all CO_2 within a melt inclusion, including both the CO_2 in the glass analyzed by ion probe, the CO_2 contained within the vapor bubble obtained by Raman spectroscopy, and the volumes of bubble and glass for each melt inclusion obtained by X-ray computed microtomography (see Table S3 for the method of reconstructing the total CO_2 content of each melt inclusion).

3. Methods for data treatment

We use a series of criteria to identify inclusions where the volatile contents have been compromised. This way the results and discussion can focus on primary magmatic signatures. Figure 2 shows all melt inclusions from which we collected volatile data. Inclusions whose volatile contents were likely compromised are designated with a black "x" in Figure 2. We do

not consider these inclusions further in our data analysis and interpretation so as to focus on primary magmatic signatures. However, one inclusion with exceptionally high Cl concentration (1.90 wt.% Cl) is included in subsequent analysis, but it is identified in all plots where it is shown.

Inclusions are excluded if they show evidence of being affected by one or more of the following:

i) *Diffusive proton loss.* Hydrogen isotopes can indicate whether H_2O loss from the melt inclusion has occurred by proton diffusion through the host olivine. Melt inclusions that have been affected by proton diffusion will have low H_2O contents and high δD values due to faster diffusion of hydrogen over deuterium (Hauri, 2002; Gaetani et al., 2012; Bucholz et al., 2013; Hartley et al., 2015). Therefore, we measured δD on all melt inclusions reported in this study. Melt inclusions in the Malumalu sample (AVON3-78-1) have a δD range of -51.8‰ to +127.6‰, and melt inclusions in the Vailulu‘u sample (AVON3-71-2) have a δD range of -52.4‰ to -22.0‰ (Figure 2). Diffusive H_2O loss from melt inclusions should produce a systematic relationship between melt inclusion δD and volume. Melt inclusions from both lavas with volumes $>10^5$ μm^3 exhibit no systematic relationship between δD and melt inclusion volume, and they exhibit a relatively narrow range in δD of -35.8±17.0‰ (2SD, N=19). However, the two melt inclusions with positive δD values, both from Malumalu (samples AVON3-78-1#13 and AVON3-78-1#32), have the smallest volumes (~8.8×10^4 μm^3 and 4.3×10^4 μm^3). Prior work has shown that smaller volume melt inclusions are more susceptible to diffusive proton loss that results in elevated δD (Hauri, 2002; Gaetani et al., 2012; Bucholz et al., 2013; Hartley et al., 2015). Therefore, the two small-volume inclusions are excluded.

ii) *Breaching.* Two melt inclusions have likely suffered breaching because CO_2 is <200 ppm and H_2O is <1 wt. % (see Figure S4; AVON3-78-1#25, AVON3-78-1#37). Both melt inclusions exhibit melt-filled cracks that intersect the melt inclusions, which is strong physical evidence that supports the breaching interpretation.

iii) *Extremely large vapor bubbles.* Three melt inclusions (AVON3-78-1#10, AVON3-78-1#28, AVON3-71-2#20) have vapor bubbles that make up >10 vol. % of the melt inclusion and are excluded. Prior work suggested that large vapor bubbles result from simultaneous entrapment of a mix of melt and CO_2 fluid (e.g. Anderson, 1974; Frezzotti, 2001; Hanyu et al., 2020; Moore et al., 2015), which is not representative of melt-only compositions.

iv) *No CO_2 detected by Raman*. No Fermi doublets were observed by Raman spectroscopy for two melt inclusions (AVON3-71-2#14, AVON3-71-2#18), thus the CO_2 densities may have been too low for detection. To err on the side of caution, we are excluding these two melt inclusions from the interpretations of this study. For other excluded melt inclusions, CO_2 densities in the vapor bubbles were highly uncertain (AVON3-71-2#20; ±0.092) or so low that negative values resulted from the calibration (AVON3-78-1#25, AVON3-78-1#37, AVON3-71-2#14), and the volatile data for these four melt inclusions are excluded from the discussion (except for AVON3-71-2#14, which has an unusually high Cl concentration and is identified in each plot where it is shown).

v) *Carbonate detected by Raman*. If carbon exists as carbonate in a melt inclusion, the CO_2 budget of the melt inclusion may be underestimated. In this study, carbonates

were detected by Raman in two Malumalu melt inclusions (AVON3-78-1#15 and AVON3-78-1#32), and volatile data for these inclusions are excluded.

4. Results

4.1 Hydrogen and strontium isotopes

After filtering the data for the compromised melt inclusions, the Samoan melt inclusions from Malumalu (-37.8±13.2‰, N=9) and Vailuluʻu (-33.9±19.7‰, N=10) are relatively homogenous in δD with an average δD value of -35.8‰ (±17.0‰, 2SD, N=19). The Samoan inclusions have heavier δD than most MORB and Lōʻihi (now known as Kamaʻehuakanaloa) values, consistent with heavy δD values (ca. -40‰) found in OIBs with recycled components (Loewen et al., 2019).

Critically, $^{87}Sr/^{86}Sr$ measurements in melt inclusions provide a test for whether the Samoan melt inclusions of this study represent the Samoan mantle sources sampled by Vailuluʻu and Malumalu glasses. If they do represent the same sources, then the volatile and trace element concentrations of the melt inclusions can be directly compared to concentration measurements in Samoan pillow lava glasses. The $^{87}Sr/^{86}Sr$ range for all of the Malumalu (sample AVON3-78-1) melt inclusions reported here is large, from 0.706594 to 0.709225 (Figure 3, 4). The inclusions largely fall within the range reported for Malumalu pillow glasses and whole rocks (0.706374–0.708901; Workman et al., 2006). The $^{87}Sr/^{86}Sr$ range for all of the Vailuluʻu (sample AVON3-71-2) melt inclusions reported here is smaller compared to AVON3-78-1 melt inclusions, from 0.704858 to 0.705718. The range of Vailuluʻu melt inclusion $^{87}Sr/^{86}Sr$ overlaps with the range reported for Vailuluʻu pillow glasses (0.705352–0.706720; Workman et al., 2006) but, relative to

Vailulu‘u pillow glasses and whole rocks, the Vailulu‘u melt inclusions are shifted to less radiogenic (lower) $^{87}Sr/^{86}Sr$ values. Taken together, the $^{87}Sr/^{86}Sr$ for the Malumalu and Vailulu‘u melt inclusions in this study bracket the $^{87}Sr/^{86}Sr$ obtained pillow glasses from each volcano: the lowest $^{87}Sr/^{86}Sr$ in the melt inclusions (0.704858) is somewhat lower than the lowest value measured in whole rocks and pillow glasses (0.705352) from these two seamounts, and the highest $^{87}Sr/^{86}Sr$ in the melt inclusions (0.709225) is slightly higher than the highest value measured in pillow glasses (0.708901). This statement is also true for the $(La/Sm)_N$ and K_2O/TiO_2 for the melt inclusions compared to the whole rocks and pillow glasses (Figure 4). Therefore, the Malumalu and Vailulu‘u melt inclusions from these two hand samples represent the full compositional range previously identified in these volcanoes and, in fact, span nearly the entire range encountered in $^{87}Sr/^{86}Sr$ (i.e., 0.7045 to 0.7089) for the eastern Samoan volcanic province—including Ta‘u, Vailulu‘u, and Malumalu volcanoes—examined by Workman et al. (2006). Thus, the melt inclusions can be used to interpret mantle source geochemical characteristics, including volatile budgets, of the volcanoes examined in Workman et al. (2006).

4.2 Volatiles

After omitting melt inclusions that have been contaminated, breached, affected by hydrogen diffusion, and have unreliable CO_2 analyses by Raman, the magmatic volatile content of the Samoan melt inclusions can be explored. Figure 5 provides ratios (H_2O/Ce, CO_2/Nb, Cl/Nb, S/Gd, and F/Nd) of volatile (H_2O, CO_2, Cl, S, and F) to nonvolatile (Ce, Nb, Gd, and Nd) incompatible trace elements (ITEs) that have similar mineral-melt partition coefficients during mantle melting and magmatic differentiation processes. Below we examine the volatile concentrations and their ratios to nonvolatile ITEs.

288 4.2.1. CO_2 in Samoan melt inclusions.

289 We use the CO_2 concentration in the melt inclusion glass analyzed by SIMS and the CO_2
290 density in the vapor bubble from Raman spectroscopy to reconstruct the total CO_2 concentration
291 of the melt inclusion. When comparing melt inclusion and vapor bubble CO_2, 3 to 94 mass
292 percent (average ~59 mass percent) of the total CO_2 (i.e., melt inclusion CO_2+vapor bubble CO_2)
293 resides in the vapor bubble, consistent with prior findings of large CO_2 fractions residing in melt
294 inclusion vapor bubbles (e.g., DeVitre et al., 2021; Aster et al., 2016; Moore et al., 2015).
295 Malumalu and Vailulu‘u melt inclusions have relatively similar total CO_2 contents of 1506–5746
296 ppm and 658–4771 ppm, respectively. The associated host pillow glasses for the Malumalu and
297 Vailulu‘u samples have total CO_2 contents of 70 ppm and 179 ppm, respectively (Workman et
298 al., 2006), which is far lower than the melt inclusions from these two volcanoes. These
299 observations are consistent with greater CO_2-H_2O saturation pressures for the melt inclusions
300 than the pillow glasses.

301 During melting and crystallization, the incompatibility (i.e., the bulk partition coefficient) of
302 CO_2 is similar to Nb and Ba, thus the ratios of CO_2/Nb or CO_2/Ba have been used to estimate
303 upper mantle carbon content (Hirschmann, 2018; Michael & Graham, 2015; Saal et al., 2002;
304 Cartigny et al., 2008; Le Voyer et al., 2017). However, only undegassed, CO_2-undersaturated
305 melts will have CO_2/Nb or CO_2/Ba that are representative of the mantle source, but such melts
306 are rare (Hauri et al., 2018; Graham & Michael, 2021; Le Voyer et al., 2017; Michael & Graham,
307 2015; Saal et al., 2002). These CO_2-undersaturated melts tend to be geochemically depleted
308 (Hauri et al., 2018; Shimizu et al., 2023) and have higher CO_2/Nb than most submarine volcanic
309 glasses, which are CO_2-saturated and thus degassed (e.g., the Samoan pillow glasses and melt
310 inclusions examined here). The Samoan melt inclusions in this study have a measured CO_2/Nb

311 range of 19 to 125 for Vailulu‘u melt inclusions and 27 to 133 for Malumalu melt inclusions, and
312 such ratios are lower than inferred for mantle sources of oceanic hotspot lavas (e.g., >1000 for
313 Iceland; Matthews et al., 2021) and MORB (CO_2/Nb > 283; Michael & Graham, 2015). Thus,
314 we suggest the Samoan samples are CO_2-saturated and degassed, which is consistent with highly
315 variable total CO_2 contents (658 to 5746 ppm) relative to the narrow range of Nb concentrations
316 in our Samoan melt inclusions (Figure S6b,d). The Samoan pillow glasses from these two
317 volcanoes have even lower (more degassed) CO_2 concentrations while exhibiting similar Nb
318 concentrations to the melt inclusions (Figure S6b,d).

319

320 4.2.2. Cl in Samoan melt inclusions versus Samoa pillow glasses.

321 Malumalu melt inclusions have 651–1198 ppm Cl, and Vailulu‘u melt inclusions have 412–
322 765 ppm Cl (excluding the high Cl inclusion AVON3-71-2#14, which has a Cl concentration of
323 1.9 wt.% Cl). The associated pillow glasses from the two samples hosting the melt inclusions—
324 AVON3-78-1 and AVON3-71-2—have 1004 ppm Cl and 1490 ppm Cl, respectively. The suite
325 of pillow glasses from all Malumalu and Vailulu‘u samples have Cl contents that vary from 886
326 to 1725 ppm and 547 to 1818 ppm, respectively.

327 To determine if any melt inclusions are influenced by the assimilation of seawater-derived
328 materials, we use Cl/Nb as an indicator of assimilation of seawater-derived materials (e.g.,
329 Kendrick et al., 2013, 2015; Kent et al., 1999a, 1999b, 2002). This is a useful ratio because Cl
330 and Nb behave similarly during crystal fractionation and melting due to their similar
331 incompatibility in basalt melts (Rowe & Lassiter, 2009). Malumalu melt inclusions have a Cl/Nb
332 range of 14–25 and Vailulu‘u melt inclusions have a Cl/Nb range of 14–22 (excluding melt

inclusion sample AVON3-71-2#14, which has with Cl/Nb = 840) (Figure 5). The Samoan melt inclusions have Cl/Nb that overlap with mid-ocean ridge basalts (MORB), where Cl/Nb_{MORB} is 5 to 17 (Lassiter et al., 2002; Le Roux et al., 2006), but the Samoan inclusions tend to be shifted to higher Cl/Nb.

The pillow glasses for the Malumalu (AVON3-78-1) and Vailulu‘u (AVON3-71-2) samples hosting the Samoan melt inclusions have Cl/Nb of 13 and 27, respectively (Kendrick et al., 2015). Both lavas have been previously suggested to have assimilated seawater-derived materials (Kendrick et al., 2014; Reinhard et al., 2018). We find some evidence for assimilation in a single melt inclusion from Vailulu‘u (AVON3-71-2#14), which has a high Cl/Nb ratio of 840, suggesting contamination by seawater-derived materials; however, any such assimilation does not appear to have impacted $^{87}Sr/^{86}Sr$ (0.705471±0.000022) as it is at the lower end of the range observed here (Figure 5).

4.2.3 S in Samoan melt inclusions versus Samoa pillow glasses.

Malumalu melt inclusions have 1786–3163 ppm S, and Vailulu‘u melt inclusions have 1582–2090 ppm S. The associated host pillow glasses (AVON3-78-1 and AVON3-71-2) have 831 ppm S and 2337 ppm S, respectively. The suite of pillow glasses from all Malumalu and Vailulu‘u samples have S contents varying from 781 to 2391 ppm and 1010 to 4834 ppm, respectively (Workman et al., 2006).

Sulfur and Gd and Dy have similar incompatibility during melting and crystal fractionation (Saal et al., 2002) when sulfide is not present, except at lower pressures when sulfur degasses. However, Samoan basalts are known to host both sulfates and sulfides (Labidi et al., 2015). The melt inclusions in this study are sulfide supersaturated (Figure S5; using the model of Fortin et

al., 2015 and Smythe et al., 2017)—and sulfides are in fact, observed in some of the inclusions from the two samples examined here —thus S/Gd (Figure 5) of Samoan melt inclusions in this study may have been influenced by sulfide saturation and are likely not representative of the Samoan primary melts.

4.2.4. F in Samoan melt inclusions versus Samoa pillow glasses.

Malumalu melt inclusions have 1161–1293 ppm F, and Vailulu‘u melt inclusions have 777–1145 ppm F. The associated host pillow glasses (AVON3-78-1 and AVON3-71-2) have 1254 ppm F and 903 ppm F, respectively. The suite of pillow glasses from all Malumalu and Vailulu‘u samples have F contents varying from 1173 to 1409 ppm, and 843 to 1188 ppm F, respectively (Workman et al., 2006).

F/Nd in melt inclusions and glasses from global datasets of MORB and OIB are suggested to be relatively constant because there is no significant F/Nd fractionation during crystallization and melting. The F/Nd values of global OIB and MORB have been estimated to be 20.1±5.8 (Workman et al., 2006), but there is evidence for greater F/Nd variability (Koleszar et al., 2009; Shimizu et al., 2016; Jackson et al., 2015; Lassiter et al., 2002; Métrich et al., 2014; Cabral et al., 2014; Rose-Koga et al., 2012). The average F/Nd for Malumalu melt inclusions (30±6 2SD, N=9) is similar to the average F/Nd for Vailulu‘u melt inclusions (29±14 2SD, N=10), but Vailulu‘u melt inclusions have more variability in F/Nd (Figure 5). Three Vailulu‘u melt inclusions (AVON3-71-2#7, #17, #22) have ~200 ppm lower F contents than the other Samoan melt inclusions, but similar Nd contents, resulting in lower F/Nd (21–23). The Samoan melt inclusion have F/Nd (29±11, 2SD, N=19) tends to be higher than the canonical F/Nd (~21) for

fresh global OIB and MORB, and higher than the average pillow glass F/Nd from Malumalu (22±2, 2SD, N=17; Workman et al., 2006) and Vailulu‘u (22±3, 2SD, N=48; Workman et al., 2006). However, the average F/Nd of Samoan melt inclusions overlaps within two standard deviations of the canonical F/Nd value and the F/Nd of Samoan pillow glasses. Nonetheless, the Vailulu‘u melt inclusions tend to very high F/Nd up to 41. Elevated F may be characteristic of the HIMU mantle source (Hauri & Hart, 1993; Rose-Koga et al., 2017; Jackson et al., 2015), and Vailulu‘u is thought to contain a small contribution from a HIMU component (Workman et al., 2004; Jackson et al., 2014). However, we do not have an explanation for the higher F/Nd in the Vailulu‘u melt inclusions relative to the glasses from this seamount.

4.2.5. H_2O in Samoan melt inclusions versus Samoa pillow glasses.

Malumalu melt inclusions have 1.56–1.95 wt.% H_2O, and Vailulu‘u melt inclusions have 1.13–1.39 wt.% H_2O. The associated host glasses from these two submarine samples tend to have lower H_2O contents than the melt inclusions with 0.91 wt.% H_2O (AVON3-78-1) and 1.18 wt.% H_2O (AVON3-71-2), respectively. The low H_2O in the AVON3-78-1 Malumalu glass sample lies within the range of H_2O for pillow glass samples from Malumalu (0.89 to 1.43 wt.%), and the same applies for the AVON3-71-2 Vailulu‘u glass sample as it also lies in the range of pillow glasses from this seamount (0.63 to 1.50 wt.%) (Figure 6). When the melt inclusions and pillow glasses are corrected for olivine fractionation to be in equilibrium with mantle olivine (Fo_{90}), a figure of H_2O_{Fo90} (wt.%) versus Ce_{Fo90} (ppm) shows that the melt inclusions and pillow glasses from Malumalu and Vailulu‘u seamounts have similar Ce_{Fo90}, but the inclusions have H_2O that is higher than the pillow glasses (Figure S6c). We also show the same plot but instead provide the

399 *measured* H_2O and Ce in the glass glasses—due to uncertainties associated with the olivine
400 correction—and find that it does not change our conclusions.

401 Consistent with this observation, the H_2O/Ce range of the Malumalu AVON3-78-1 melt
402 inclusions (149–232, average 193±47, 2SD, N=10) and the Vailulu‘u AVON3-71-2 melt
403 inclusions (161–275, average 190±78, 2SD, N=10) are higher than the host pillow glasses, 59
404 (for pillow glass from sample AVON3-78-1) and 123 (for pillow glass from sample AVON3-71-
405 2), respectively. Critically, the average H_2O/Ce (197±58 2SD, N=15) in the melt inclusion
406 dataset from Malumalu and Vailulu‘u seamounts is nearly twice as high as the same ratio in the
407 Samoan pillow glasses from these two seamounts (106±51, 2SD, N=65). This is notable because
408 the inclusions and pillow glasses are from the same two volcanoes, span the same range of
409 $^{87}Sr/^{86}Sr$ (Figure 3), and have similar ITE ratios (Figure 4), suggesting they sample the same
410 mantle sources. This observation that melt inclusions have higher H_2O/Ce than submarine pillow
411 glasses may relate to the fact that the Samoan melt inclusions from Malumalu and Vailulu‘u
412 have universally higher calculated MagmaSat CO_2-H_2O vapor saturation pressures (Figure 3)
413 than the submarine pillow glasses, reflective of higher entrapment pressures for the melt
414 inclusions (>0.870 kbar) than the eruption pressures experienced by the glasses (<0.53 kbar) (see
415 Figure 3).

416 While Workman et al. (2006) found a negative correlation between H_2O/La and $^{87}Sr/^{86}Sr$ for
417 Samoan glasses, we find that the Samoan melt inclusions in this study exhibit *no correlation*
418 between H_2O/Ce and $^{87}Sr/^{86}Sr$ (Figure 3, 5a, 7a), even though the melt inclusions are from two of
419 the three volcanoes studied by Workman et al. (2006) and span the same range of $^{87}Sr/^{86}Sr$ as
420 their pillow glasses. In contrast to Workman et al. (2006), the H_2O/Ce of the melt inclusions is
421 quite constant (i.e., 197±58 2SD, N=15) over a range of $^{87}Sr/^{86}Sr$ from 0.704858 to 0.709225,

and the melt inclusions with the strongest EM2 mantle signatures (i.e., $^{87}Sr/^{86}Sr > 0.7080$, N=4) have elevated H_2O/Ce (193±19 2SD) that is indistinguishable from the H_2O/Ce (202±31) in melt inclusions with weaker EM2 signatures ($^{87}Sr/^{86}Sr < 0.7080$, N=3).

While the Samoan pillow glasses and melt inclusions exhibit some overlap with each other in H_2O/Ce at the lowest $^{87}Sr/^{86}Sr$, they exhibit diverging trends in H_2O/Ce with increasing $^{87}Sr/^{86}Sr$: melt inclusions exhibit unchanging H_2O/Ce with increasing $^{87}Sr/^{86}Sr$, and glass exhibit decreasing H_2O/Ce with increasing $^{87}Sr/^{86}Sr$. Thus, the difference in H_2O/Ce between melt inclusions and glasses is largest at the highest $^{87}Sr/^{86}Sr$ (Figure 7). To illustrate this, we note that all four pillow glasses with the strongest EM2 signatures ($^{87}Sr/^{86}Sr > 0.7080$) have $H_2O/Ce < 90$ (H_2O/Ce average of 75±30, 2SD) while the H_2O/Ce of the four melt inclusions with the highest $^{87}Sr/^{86}Sr$ (>0.7080) have H_2O/Ce that is more than twice as high as that in the pillow glasses (H_2O/Ce average of 193±19, 2SD). Prior studies (e.g., Workman et al., 2006) often cite that pillow glasses erupted at depths >1000 mbsl retain volatile/ITE ratios of the mantle source. All pillow glasses shown in Figure 7 have H_2O-CO_2 saturation pressures ≥0.1 kbar. Given that the melt inclusions and glasses in Figure 7 exhibit deep saturation pressures and appear to sample the same mantle source (Figure 4), we might expect the deeply-erupted pillow glasses should have the same H_2O/Ce as melt inclusions. These observations raise a key question that we will address in the discussion: why do melt inclusions and pillow glasses erupted at depths >1000 mbsl from the same volcanoes and with the same $^{87}Sr/^{86}Sr$ (i.e., sampling the same mantle sources) have H_2O/Ce that differ, on average, by nearly a factor of two?

5. Modeling degassing processes for Samoan melts

444 We find that melt inclusions from the Vailulu‘u and Malumalu seamounts have higher
445 CO_2 concentrations than their corresponding pillow glasses (Figure 6), indicating that the deeply-
446 erupted submarine pillow glasses are more degassed than the melt inclusions. An outstanding
447 question is whether the lower H_2O/Ce in the pillow glasses reflects this higher degree of
448 degassing via concomitant degassing of both CO_2 *and* H_2O.

449 We show that the data are consistent with Samoan pillow glasses being related to the
450 Samoan melt inclusions through closed-system degassing; the new insight gained here is that,
451 when compared with genetically-related melt inclusions, it is clear that even deeply erupted
452 glasses (with CO_2-H_2O saturation pressures ≥0.1 kbar) have lost significant H_2O and have lower
453 H_2O/Ce compared to their primary melt (Figure 3). This is evident in models we have run using a
454 set of open- and closed-system degassing paths while also varying the fraction of CO_2+H_2O fluid
455 in equilibrium with the initial melt (Figure 6). In the models, we define the variable M as the
456 percentage of fluid in equilibrium with the melt, where M = 0% means that no initial fluid is in
457 equilibrium with the melt (i.e., all volatiles are dissolved in the melt, no fluid is present), and
458 where M = 100% means that all volatiles are in the fluid (i.e., no melt is present). The higher the
459 M value, the deeper degassing starts. We generate degassing paths assuming a starting H_2O and
460 CO_2 composition equivalent to the melt inclusion with the highest H_2O content from Malumalu
461 seamount (sample AVON3-78-1#3) to model Malumalu data, and the equivalent high-H_2O melt
462 inclusion from Vailulu‘u (sample AVON3-71-2#10) to model Vailulu‘u data. We use MagmaSat
463 (Ghiorso & Gualda, 2015) to calculate the fluid composition (i.e., $X$$CO_2$ and $X$$H_2O$) in
464 equilibrium with the two melt inclusions (see Table S9 for model melt inclusion compositions).
465 Additionally, we use rhyolite-MELTS v.1.2 (which incorporates the same fluid solubility model
466 as MagmaSat) to simulate degassing because this model is well-suited for high CO_2 contents in

the initial melt composition (Ghiorso & Gualda, 2015; Gualda et al., 2012). The models are run at 1200 °C, and start at 7–15 kbar (for Malumalu degassing paths, due to higher initial CO_2 contents), or 7 kbar (for Vailulu‘u, which has lower initial CO_2), and run to 1 bar. The influence of oxygen fugacity on the model degassing path is negligible, so we assume QFM for all models. The compositional and physical parameters used in the MagmaSat and rhyolite-MELTS models are given in Table S9.

The degassing model results are presented in Figure 6. While there is no single degassing path that explains the difference in pillow glass and melt inclusion CO_2 and H_2O concentrations, closed-system degassing paths with M values ranging from 0% to 10% describe most of the pillow glasses from both seamounts. However, there are some Vailulu‘u pillow glasses that have H_2O that is higher than the range described by the calculated degassing paths. For example, three Vailulu‘u pillow glasses have higher H_2O concentrations than the highest-H_2O melt inclusion. This could be because the melt inclusion suite in this study does not represent the full range of H_2O contents possible at the seamount, and higher initial H_2O concentrations may be more reflective of the primary melts.

A primary observation from this modeling exercise is that closed-system degassing from melt inclusion entrapment pressures (i.e., >0.87 kbar) to eruption on the seafloor (pillow glasses have equilibrium pressures of 0.08 to 0.53 kbar) results in significant loss of both CO_2 *and* H_2O, even for glasses with CO_2-H_2O saturation depths near 0.4 kbar (see closed-system degassing paths in Figure 6). Furthermore, the presence of equilibrium fluid (M) indicates that the magmatic system is richer in CO_2, and thus starts to degas at greater depths. Below we show that loss of H_2O during closed-system degassing to shallow levels (i.e., <0.53 kbar) explains the lower H_2O/Ce in pillow glasses compared to the melt inclusions.

6. Discussion

H_2O has incompatibility during mantle melting similar Ce (Michael, 1995), thus H_2O/Ce of the melt inclusions and glasses should reflect the mantle source unless the samples have degassed. Clear negative correlations between H_2O/Ce and $^{87}Sr/^{86}Sr$ in pillow glasses have been used to infer the H_2O/LREE (light rare earth element) ratios of the mantle source, assuming the H_2O has not been degassed. The primary observation in this study that we seek to explain is that Samoan pillow glasses and olivine-hosted melt inclusions span the same range of $^{87}Sr/^{86}Sr$ and trace element ratios—and thus sample the same mantle sources, yet the melt inclusions have H_2O/Ce ratios that are approximately twice as high as the pillow glasses. The second key observation is that the melt inclusion H_2O/Ce ratios are relatively constant over a wide range of $^{87}Sr/^{86}Sr$, in contrast to the pillow glasses whose H_2O/Ce ratios anticorrelate with $^{87}Sr/^{86}Sr$. This raises two key questions: Why do Samoan EM2 pillow glasses exhibit H_2O/Ce that are approximately half the values in Samoan EM2 melt inclusions at the same seamounts, and what does this mean for the H_2O content of the EM2 mantle?

6.1. Higher H_2O/Ce in melt inclusions relative to pillow glasses: Diffusive H_2O gain through host olivine and/or assimilation of seawater-derived materials?

In order to compare the volatile contents of the Samoan melt inclusions and pillow glasses in this study, it is important to assess whether the higher H_2O/Ce in the inclusions reflects processes operating in the magma during ascent, such as diffusive proton gain (i.e., addition of H) or assimilation of seawater-derived materials. Prior work has shown that, compared to large melt inclusions, small inclusions are more susceptible to diffusive loss or addition of protons,

and this results in modified δD (Hauri, 2002; Portnyagin et al., 2008; Gaetani et al., 2012; Bucholz et al., 2013; Hartley et al., 2015). Given enough time, the δD of all inclusions will eventually equilibrate with the external melt. Diffusive proton loss from the inclusion can be identified by an increase in δD, which is associated with decreasing melt inclusion volume. Conversely, diffusive gain of protons by the inclusion is identified by a decrease in δD, where the magnitude of the δD reduction is greater in the smaller volume melt inclusions. The new δD analyses on melt inclusions show a lack of variation in δD (-35.8±17.0‰, 2SD, N=19) with melt inclusion size for melt inclusions with volumes $>10^5$ μm^3, which indicates no water loss or gain in the larger inclusions (Figure 2). However, the two smallest melt inclusions (AVON3-78-1#13 and AVON3-78-1#32), both with melt inclusion volume $<10^5$ μm^3, have significantly higher δD (+128‰ and +6 ‰, respectively) than the other melt inclusions from this lava, which indicates that the small volume melt inclusions have experienced diffusive H_2O loss, not H_2O addition (Figure 2). These two small volume inclusions are excluded from the discussion below.

Assimilation of seawater-derived materials can increase H_2O in magmas (except if the magma is saturated in H_2O), and this process can be traced by monitoring Cl/Nb, a ratio that is elevated in seawater-derived materials. One hypothesis for the higher H_2O/Ce in melt inclusions is that they have experienced more assimilation of seawater-derived materials compared to Samoan pillow glasses, and this hypothesis can be tested by measurement of $^{87}Sr/^{86}Sr$. A plot of Cl/Nb versus $^{87}Sr/^{86}Sr$ shows that Samoan pillow glasses and melt inclusions have an overlapping range of Cl/Nb at any given $^{87}Sr/^{86}Sr$, so the offset to higher H_2O/Ce in the melt inclusions is not explained by greater assimilation experienced by melt inclusions (Figure 5). We do acknowledge that one melt inclusion with exceptionally high Cl/Nb (840)—a ratio consistent with assimilation of seawater-derived materials (Table S1)—also has elevated H_2O/Ce (366),

535 suggesting a role for assimilation in increasing the H_2O/Ce in this particular inclusion. However,
536 this single inclusion has been excluded from the discussion below owing to its very high Cl/Nb.

537 In short, diffusive gain of H_2O and preferential assimilation of seawater-derived materials
538 by the melt inclusions relative to the pillow glasses do not explain the higher H_2O/Ce in the melt
539 inclusions relative to the pillow glasses. Instead, we argue in the following section that closed-
540 system degassing plays a key role in lowering the H_2O and the H_2O/Ce of pillow glasses. In
541 contrast, limited H_2O degassing has occurred in the melt inclusions in this study, leaving the melt
542 inclusion H_2O/Ce relatively unchanged, thereby explaining why melt inclusions have higher
543 H_2O/Ce than pillow glasses. This contrasts with prior studies (e.g., Workman et al., 2006)
544 suggesting that pillow glasses erupted at depths >1000 mbsl retain H_2O/LREE ratios of the
545 mantle source.

546 **6.2 Higher H_2O/Ce in melt inclusions relative to pillow glasses: H_2O loss in Samoan glasses**
547 **caused by degassing**

548 We argue that the difference in H_2O/Ce between Samoan EM2-flavored melt inclusions
549 and pillow glasses from the same seamounts relates to greater degassing of the pillow glasses
550 relative to the melt inclusions. Unlike the pillow glasses, which can experience degassing from
551 great depth all the way to eruption and quenching on the seafloor, melt inclusions trap melts at
552 magma chamber depths and act as pressure vessels, which inhibits degassing at shallower levels
553 during magma ascent. To evaluate this hypothesis, we build on the indistinguishable $^{87}Sr/^{86}Sr$
554 and nonvolatile incompatible trace element ratios between pillow glasses and melt inclusions and
555 argue that, at the depth of melt inclusion entrapment, the H_2O/Ce of the melts that later erupted
556 as Samoan pillow glasses was *also* the same as the Samoan melt inclusions (i.e., nonvolatile ITE
557 ratios—which remain unmodified from primary melt compositions during fractional

crystallization of magmas with MgO as high as identified in the data reported here (Figure S1)—and $^{87}Sr/^{86}Sr$ data obtained on the melt inclusions indicate that they derive from the same parental melts as the pillow glasses and thus should have started with the same H_2O/Ce). The H_2O/Ce of the pillow glasses, but not the melt inclusions, was then lowered by H_2O degassing during ascent.

The hypothesis of H_2O loss from the matrix melts by degassing is supported by closed-system degassing models in Figure 6. For example, the degassing model for Malumalu AVON3-78-1 starts with a melt inclusion composition like AVON3-78-1#3 which has an elevated CO_2 concentration of 2810 ppm, the highest H_2O concentration from this lava (1.95 wt.%), and a high entrapment pressure of 2.63 kbar (i.e., the CO_2-H_2O saturation pressure calculated for the melt inclusion using MagmaSat). Closed-system degassing of this melt composition from 2.63 kbar to 0.2 kbar—the approximate CO_2-H_2O saturation pressure for the pillow glass from this lava, sample AVON3-78-1—at M=1.6 lowers the water content by a factor of ~2.1 to 0.90 wt.%, and the CO_2 content by a factor of ~40 to 69 ppm. The red "x" in Figure 6a defines the CO_2 and H_2O composition of the model melt following degassing, and the degassed model melt is very similar in composition to the pillow glass sample AVON3-78-1 and helps explain the low H_2O (0.91 wt.%) and CO_2 (70 ppm) of AVON3-78-1. This is important because this particular pillow glass sample anchors the highest $^{87}Sr/^{86}Sr$ (0.7089) and lowest H_2O/Ce (59) portion of the $^{87}Sr/^{86}Sr$ versus H_2O/Ce array produced by Workman et al. (2006) who interpreted that the low H_2O/Ce in this EM2 glass reflects melting of a water-poor ("dry") EM2 mantle. In contrast, we show that dramatic H_2O-loss during closed-system degassing of an ascending EM2 melt with an initially high H_2O/Ce ratio (H_2O/Ce = 200) is responsible for the low H_2O/Ce (59) in the AVON3-78-1 glass. This model contrasts with prior studies (e.g., Workman et al., 2006) suggesting that pillow

glasses erupted at depths >1000 mbsl (≥0.1 kbar) retain the H_2O/LREE ratios of the mantle source.

We observe a relatively constant and elevated H_2O/Ce ratio in melt inclusions over a wide range of $^{87}Sr/^{86}Sr$—melt inclusions with strong EM2 mantle signatures (i.e., $^{87}Sr/^{86}Sr > 0.7080$) have elevated H_2O/Ce (193±19 2SD, N=4) that is indistinguishable from H_2O/Ce (202±31, N=3) in melt inclusions with weaker EM2 signatures ($^{87}Sr/^{86}Sr < 0.7080$). This also contrasts with Workman et al.'s (2006) observation that H_2O/LREE is lower in the Samoan EM2 pillow glasses with higher $^{87}Sr/^{86}Sr$. Unlike Workman et al. (2006), who argued that the low H_2O/LREE in Samoan EM2 glasses is a source feature, we show that the low ratio in these pillow glasses relative to that of the melt inclusions can be explained by closed-system degassing of magmas during ascent to the seafloor. If this degassing model is correct, and if Samoan high $^{87}Sr/^{86}Sr$ and low $^{87}Sr/^{86}Sr$ melts have the same initial H_2O/Ce—as supported by observations from melt inclusions in Figure 5a—then the negative correlation between $^{87}Sr/^{86}Sr$ in H_2O/Ce in the pillow glasses in Workman et al. (2006) (Figure 7) leads us to an important conclusion: the Samoan EM2 pillow glasses have degassed more H_2O (to achieve lower H_2O/Ce) than Samoan pillow glasses with weaker EM2 signatures (which have higher H_2O/Ce). Therefore, we next focus on identifying the mechanism that results in greater H_2O degassing in more extreme EM melts relative to non-EM melts.

6.3 Explaining the inverse relationship between $^{87}Sr/^{86}Sr$ and H_2O/Ce in global pillow glasses by degassing.

The global OIB dataset on submarine pillow glasses exhibits an inverse relationship between $^{87}Sr/^{86}Sr$ and H_2O/Ce (Figure 7) that is similar to the inverse correlation observed in

Samoan submarine glasses, and it has long been known that submarine glasses with low $^{87}Sr/^{86}Sr$ tend to have higher H_2O/Ce than glasses with high $^{87}Sr/^{86}Sr$ (e.g., Dixon et al., 2002; Workman et al., 2006; Kendrick et al., 2014). The Samoan melt inclusions noticeably stray from this trend. The Samoan melt inclusions with high $^{87}Sr/^{86}Sr$ are shifted to higher, relatively constant H_2O/Ce (197±58 2SD, N=15) compared to the H_2O/Ce (108±58, 2SD, N=41) in a global database of OIB glasses (including Samoa) that have similarly high $^{87}Sr/^{86}Sr$ (i.e., >0.7037) (Figure 7). In fact, the high H_2O/Ce of Samoan inclusions (197±58 2SD, N=15) is similar to the H_2O/Ce (209±92, 2SD, N=32) of pillow glasses characterized by low $^{87}Sr/^{86}Sr$ (<0.7037, the threshold value used to distinguish between EM and non-EM melts). If the Samoan melt inclusions represent less degassed versions of the melts sampled by Samoan submarine glasses, then the similarity in H_2O/Ce between low $^{87}Sr/^{86}Sr$ (<0.7037) OIB pillow glasses and Samoan melt inclusions (>0.7037) raises the possibility that non-EM OIB melts and EM OIB melts initially have the same H_2O/Ce, but the latter suffer more degassing of H_2O than the former during magma ascent. If the inverse correlation between H_2O/Ce and $^{87}Sr/^{86}Sr$ in Samoan, and global, OIB glasses is driven by greater degassing of the most geochemically enriched lavas compared to geochemically depleted lavas, what mechanism causes geochemically enriched glasses from OIB mantle sources to have suffered more H_2O degassing than geochemically depleted glasses?

Previous work suggests that EM mantle sources have higher CO_2, and generate primary melts with higher CO_2, than non-EM mantle sources (Burnard et al., 2014; Cartigny et al., 2008; Taracsák et al., 2019; Hauri et al., 2018; Miller et al 2019; Matthews et al. 2021; Michael & Graham, 2015; Shimizu et al., 2023). We show that primary melts with higher CO_2 degas more CO_2 *and* more H_2O by closed-system degassing during ascent than primary melts with the same H_2O but lower CO_2 concentrations. As a result, EM lavas that were initially more CO_2-rich erupt

on the seafloor with lower H_2O/Ce than their geochemically-depleted non-EM counterparts that started with lower primary melt CO_2, even though both EM and non-EM primary melts started with the same H_2O concentrations and H_2O/Ce. At the extreme end, non-EM (i.e., geochemically depleted) melts erupted at, for example, MORB settings, can have such low primary melt CO_2 that they never saturate and neither CO_2 nor H_2O are lost by degassing (Saal et al., 2002; Michael & Graham, 2015; Hauri et al., 2018).

By contrast, we argue that CO_2-rich primary melts, typical of geochemically-enriched OIB settings, saturate CO_2 at great depths and lose significant CO_2 and H_2O by closed-system degassing. In order to show this, we first estimate primary melt CO_2 for a suite of global OIB glasses using a set of relationships shown in Figures 8 and 9. Because OIB glasses are degassed in CO_2 to variable degrees, we estimate primary melt (undegassed) CO_2 for OIB glasses in the following way. First, using a new correlation between undegassed CO_2/Nb and $(La/Sm)_N$ in MORB and OIB (see equation in Figure 9a and discussion in Supplementary Information section S1.8), together with the measured $(La/Sm)_N$ available in the suite of OIB glasses examined here, we can calculate the primary melt CO_2/Nb in the OIB glasses (Figure 8c). (It is worth noting that the correlation between CO_2/Nb and $(La/Sm)_N$ in Figure 9a is similar to a relationship previously suggested for MORB by Cartigny et al. (2008) (Figure 9b).) We then calculate the primary melt Nb concentrations for each of the OIB glasses by correcting for olivine addition or subtraction so the melts are in equilibrium with mantle (Fo_{90}) olivine (Figure 8d). By multiplying calculated primary melt CO_2/Nb (Figure 8c) by the calculated primary melt Nb concentrations (Figure 8d), we obtain primary melt CO_2 concentrations for the OIB glasses (Figure 8e). These calculations suggest that the most extreme EM OIB glasses (which have the lowest H_2O/Ce)—all from the Samoa, Societies, and Pitcairn hotspots—tend to have the highest primary melt CO_2 (Figure 8e),

650 with CO_2 concentrations commonly as high as 5 to 6 wt.% in Samoa and Societies lavas (and
651 higher than 80,000 ppm CO_2 in two Samoan lavas). These high OIB primary melt CO_2
652 concentrations calculated with our new model are in broad agreement with CO_2 concentrations
653 calculated using the petrologic model of Sun and Dasgupta (2020) (see supplementary Figure S9
654 for direct comparison).

655 Based on these calculations, Samoan primary melts inferred from the pillow rim glass
656 data have CO_2 concentrations between ~28,000 ppm and ~94,000 ppm, with most values
657 clustering near ~60,000 ppm CO_2 (Figure 8e). With few exceptions, the non-EM OIB (which
658 have the highest erupted H_2O/Ce)—Lō‘ihi, Easter, and Foundation—have lower calculated
659 primary melt CO_2 than the EM OIB—Samoa, Societies, Pitcairn, and Réunion (Figure 8e). This
660 is consistent with prior suggestions that geochemically enriched mantle domains with higher
661 $^{87}Sr/^{86}Sr$ generate primary melts with higher CO_2 than geochemically depleted mantle domains
662 (Burnard et al., 2014; Cartigny et al., 2008). Like Burnard et al. (2014), we argue that melts with
663 higher initial CO_2—characteristic of EM melts (Figure 8e)—undergo greater degrees of
664 degassing than melts with lower initial CO_2. We then show that, everything else being the same,
665 higher initial CO_2 melts experience greater degassing of H_2O (and thus have lower erupted
666 H_2O/Ce) than melts with lower initial CO_2 (Figure 8).

667 In order to demonstrate this quantitatively, we use the calculated primary melt CO_2 of the
668 OIB glasses in Figure 8e, as well as estimated primary melt H_2O (see below), as inputs to a
669 closed-system degassing model. We then show that the CO_2-rich (60,000 ppm) model primary
670 melt degasses by closed-system degassing to have H_2O concentration and H_2O/Ce similar to
671 values measured in Samoan EM pillow glasses. To test our hypothesis that high primary melt
672 CO_2 concentrations results in more degassing of H_2O, and thus, lower H_2O/Ce in the final

673 erupted and degassed melt, we examine how H_2O and CO_2 concentrations change with
674 decreasing pressure starting with two hypothetical primary melts that are identical in all respects
675 except for the initial CO_2 concentrations: the two melt endmembers are given the same starting
676 H_2O (2 wt.%), H_2O/Ce (200), and major and trace element chemistry (see compositions in Table
677 S9). The first model melt is assigned a higher CO_2 concentration of 60,000 ppm, meant to
678 approximate the elevated CO_2 concentration of EM glasses in Figure 8e (see previous
679 paragraph), and comes from our new model for calculating CO_2 in OIB primary melts (Figure
680 8c, 9a) for which calculated Samoan primary melt CO_2 concentrations tend to cluster near 60,000
681 ppm CO_2. The second model melt is assigned an initial CO_2 concentration of 5,000 ppm, and is
682 meant to approximate the CO_2 concentration of the non-EM glasses from Foundation, Easter,
683 and Lō‘ihi in Figure 8e. In order to illustrate the impact of H_2O loss during degassing as a
684 function of initial primary melt CO_2 concentration, we model the closed-system degassing paths
685 of the two melts using rhyolite-MELTS. Degassing of the high CO_2 (60,000 ppm) melt starts at
686 26 kbar (i.e., where CO_2 first saturates; see dark green line in Figure 10), which is higher than the
687 4 kbar pressure where the lower CO_2 melt saturates (see light green line in Figure 10). After both
688 the high- and low-CO_2 melts degas to the same low eruptive pressure (Figure 10)—0.5 kbar,
689 meant to represent pressure for eruption on the seafloor at ~5000 mbsl—the high CO_2 melt has a
690 significantly lower H_2O concentration and lower H_2O/Ce (~0.94 wt.% and 94, respectively)
691 compared to the low CO_2 melt (~1.56 wt.% wt.% and 156, respectively), even though both melts
692 started with the same H_2O (2 wt.%) and H_2O/Ce (200). In summary, a melt with initial CO_2 of
693 60,000 ppm degases nearly 53% of its H_2O (and 99.4% of its CO_2) during ascent to 0.5 kbar, but
694 the melt with 5000 ppm initial CO_2 degases just 22% of its H_2O (and 96.8% of its CO_2) during

695 ascent to 0.5 kbar. Thus, everything else being the same, high CO_2 melts degas more H_2O and
696 have lower H_2O/Ce than low CO_2 melts.

697 The simple degassing model in Figure 10 helps explain the observation that EM pillow
698 glasses erupted on the seafloor have lower H_2O/Ce compared to non-EM pillow glasses: EM
699 primary melts, which are associated with higher initial CO_2 (Figure 8e), saturate in volatiles
700 deeper in the crust/mantle and degas more CO_2 and H_2O prior to eruption than non-EM melts
701 with lower primary melt CO_2. The Samoan melt inclusions in this study exhibit high H_2O/Ce,
702 similar to non-EM melts, because CO_2 and H_2O degassing was arrested following melt inclusion
703 entrapment in olivine at high pressures (0.870 to 5.13 kbar). Although the Samoan melt
704 inclusions lost significant amounts of CO_2 prior to being entrapped by olivine, these melt
705 inclusions still preserve higher H_2O/Ce than the erupted pillow glasses due to having degassed
706 less CO_2 and, thus, less H_2O. However, we acknowledge that, prior to entrapment, even the melt
707 inclusions may have already lost some H_2O due to concomitant loss of both H_2O and CO_2 during
708 closed-system degassing. Nonetheless, melt inclusions preserve higher H_2O and H_2O/Ce than
709 pillow glasses, and thus preserve values closer to the primary melts.

710 **6.4 Comparison with prior models for the origin of low H_2O/Ce in EM lavas, and**
711 **implications for a "damp" EM mantle.**

712 Previous studies have suggested that the negative correlation between H_2O/Ce and
713 $^{87}Sr/^{86}Sr$ is the result of dehydration (H_2O depletion) in the EM source, which has low H_2O/Ce
714 that gives rise to EM primary melts with low H_2O/Ce. In these models, the EM mantle source
715 has low H_2O/Ce because subducted materials contributing to the EM mantle lose H_2O during
716 subduction (Dixon et al., 2002) or via diffusion during residence in the mantle (Workman et al.,
717 2006), or because the pyroxenite—which has low H_2O/Ce—contributes to the EM mantle

718 (Bizimis & Peslier et al., 2015). However, if these models explained the origin of the low
719 H_2O/Ce in high $^{87}Sr/^{86}Sr$ glasses from Samoa, then the Samoan melt inclusions with high
720 $^{87}Sr/^{86}Sr$ should also exhibit lower H_2O/Ce, but this is not the case.

721 Thus, an important implication is that submarine glasses cannot be reliably used to
722 estimate the H_2O/Ce content of OIB primary melts, particularly glasses for EM OIB that appear
723 to experience greater degassing (owing to higher initial CO_2) than non-EM OIB. Our data show
724 that, unlike Samoan submarine glasses, Samoan melt inclusions have similar H_2O/Ce (197±58,
725 2SD, N=15) that does not vary with $^{87}Sr/^{86}Sr$. In fact, the H_2O/Ce ratio (193±19, 2SD, N=4) for
726 extreme Samoan EM2 ($^{87}Sr/^{86}Sr > 0.708$) melt inclusions overlaps with H_2O/Ce suggested for
727 depleted mantle domains that are sampled by non-EM OIB ($^{87}Sr/^{86}Sr<0.7037$; H_2O/Ce =
728 209±92), average Pacific MORB (180±20; Dixon et al., 2017), average depleted N. Atlantic
729 MORB (230±20; Dixon et al., 2017), and PREMA (*Pre*valent *Ma*ntle) Pacific and Atlantic OIB
730 (215±30 and 220±30, respectively, where PREMA-type OIB do not bear EM or HIMU
731 signatures; Dixon et al., 2017). Thus, the major implication of this work is that, instead of being
732 "dry", the EM2 mantle sampled by Samoa is just as "damp" as non-EM reservoirs, but this can
733 only be seen by examining deeply entrapped melt inclusions that preserve higher CO_2 and H_2O
734 than submarine pillow glasses. Due to pronounced CO_2 and concomitant H_2O degassing that
735 appears to impact enriched lavas more than depleted ones—owing to higher primary melt CO_2 in
736 the former relative to the latter—future melt inclusion studies will be important for determining
737 the initial H_2O/Ce in EM1 (Pitcairn) and other EM2 (Societies) lavas, where existing low
738 H_2O/Ce values measured in high $^{87}Sr/^{86}Sr$ Pitcairn and Societies submarine glasses (Kendrick et
739 al. 2014) may also be due to the same degassing mechanism that lowers H_2O/Ce in Samoan OIB.
740 If so, H_2O/Ce in the mantle is not likely to be as variable as previously supposed, and much of

741 the mantle sampled by MORB and OIB have very similar H_2O/Ce that is, on average, close to a
742 value of 200, and not as low as values found in pillow glasses of EM lavas (down to 59 in
743 Samoan pillow glasses, 86 in Societies glasses, and 95 in Pitcairn glasses). Thus, like the Pb/Ce
744 ratio, which is similar in OIB and MORB globally (Hofmann et al., 1986), the H_2O/Ce ratio may
745 also be similar in the sources of plume-derived lavas (Michael, 1995).

746 A second implication of "damp" H_2O/Ce in EM Samoan lavas is that, in spite of hosting
747 subducted continental materials which have presumably lost H_2O by degassing at an ancient
748 subduction zone (White & Hofmann, 1982; Farley et al., 1992; Jackson et al., 2007), Samoan
749 EM2 melt (as sampled by EM melt inclusions) do not have lower H_2O/Ce than non-EM OIBs.
750 This is a surprising result, and suggests that recycled continental materials may not play a large
751 role in governing the H_2O budgets of mantle domains. This could be because the amount of
752 recycled continental crust in the mantle sources of OIB is small, and thus has a diminished
753 impact on the overall H_2O and H_2O/Ce of the mantle source. For example, Samoan lava
754 AVON3-78-1 examined in this study, which has a strong EM2 signature ($^{87}Sr/^{86}Sr$ of 0.7089), is
755 estimated to have only ~1% continental crust (Reinhard et al., 2018) that is added to a depleted
756 plume component that constitutes the rest (99%) of the mantle source. In this model, the H_2O and
757 Ce budgets of the EM2 mantle source is primarily controlled by the depleted plume component,
758 even if the recycled continental crust component has low H_2O/Ce. In this way, both depleted
759 mantle and EM OIB can have similar H_2O/Ce.

760

761 **Acknowledgements:** MGJ gratefully acknowledges being wrong (and that John Lassiter was
762 correct) in the debate about whether mantle source H_2O/Ce is preserved in deeply dredged
763 (>1000 mbsl) submarine pillow glasses. OEA thanks Marc Hirschmann for a discussion about

CO_2/Nb in oceanic lavas, Gareth Seward for his skillful assistance with UCSB's electron microprobe, Jean-Luc Devidal for assisting EFR-K with LA-ICP-MS analyses, and Brian Monteleone for his time and help with ion probe analyses. MGJ acknowledges NSF grants OCE-1736984, EAR-1900652, OCE-1912931, and OCE-1929095 that supported this work.

References cited

Adams, J.V., Spera, F.J. and Jackson, M.G. (2021). Trachytic melt inclusions hosted in clinopyroxene offer a glimpse into Samoan EM2-endmember melts. *Geochemistry, Geophysics, Geosystems*, *22*(3), p.e2020GC009212. https://doi.org/10.1029/2020GC009212

Anderson, A.T. (1974). Evidence for a picritic, volatile-rich magma beneath Mt. Shasta, California. *Journal of Petrology*, 15, 243–267. https://doi.org/10.1093/petrology/15.2.243

Anderson, K. R., & Poland, M. P. (2017). Abundant carbon in the mantle beneath Hawai'i. *Nature Geoscience*, 10(9), 704–708. https://doi.org/10.1038/ngeo3007

Anderson, O.E., Jackson, M.G., Rose-Koga, E.F., Marske, J.P., Peterson, M.E., Price, A.A., Byerly, B.L. and Reinhard, A.A. (2021). Testing the recycled gabbro hypothesis for the origin of "ghost plagioclase" melt signatures using $^{87}Sr/^{86}Sr$ of individual olivine-hosted melt inclusions from Hawai'i. *Geochemistry, Geophysics, Geosystems*, *22*(4). https://doi.org/10.1029/2020GC009260

Aiuppa, A., Casetta, F., Coltorti, M., Stagno, V., & Tamburello, G. (2021). Carbon concentration increases with depth of melting in Earth's upper mantle. *Nature Geoscience*, *14*(9), 697–703. https://doi.org/10.1038/s41561-021-00797-y

Asimow, P. D., & Langmuir, A. C. (2003). The importance of water to oceanic mantle melting regimes. *Nature*, *421*(6925), 815–820. https://doi.org/10.1038/nature01429

Aster, E. M., Wallace, P. J., Moore, L. R., Watkins, J., Gazel, E., & Bodnar, R. J. (2016). Reconstructing CO_2 concentrations in basaltic melt inclusions using Raman analysis of vapor bubbles. *Journal of Volcanology and Geothermal Research*, 323, 148–162. https://doi.org/10.1016/j.jvolgeores.2016.04.028

Aubaud, C. (2022). Carbon stable isotope constraints on CO_2 degassing models of ridge, hotspot and arc magmas. *Chemical Geology*, *605*, 120962. https://doi.org/10.1016/j.chemgeo.2022.120962

Bizimis, M., & Peslier, A. H. (2015). Water in Hawaiian garnet pyroxenites: Implications for water heterogeneity in the mantle. *Chemical Geology*, *397*, 61–75. https://doi.org/10.1016/j.chemgeo.2015.01.008

Boudoire, G., Rizzo, A. L., Di Muro, A., Grassa, F., & Liuzzo, M. (2018). Extensive CO_2 degassing in the upper mantle beneath oceanic basaltic volcanoes: First insights from Piton de la Fournaise volcano (La

Réunion Island). *Geochimica et Cosmochimica Acta*, *235*, 376–401. https://doi.org/10.1016/j.gca.2018.06.004

Bucholz, C. E., Gaetani, G. A., Behn, M. D., & Shimizu, N. (2013). Post-entrapment modification of volatiles and oxygen fugacity in olivine-hosted melt inclusions. *Earth and Planetary Science Letters*, *374*, 145–155. https://doi.org/10.1016/j.epsl.2013.05.033

Burnard, P., Reisberg, L., & Colin, A. (2014). An observed link between lithophile compositions and degassing of volatiles (He, Ar, CO_2) in MORBs with implications for Re volatility and the mantle C/Nb ratio. *Earth and Planetary Science Letters*, *395*, 159–167. https://doi.org/10.1016/j.epsl.2014.03.045

Cabral, R.A., Jackson, M.G., Koga, K.T., Rose-Koga, E.F., Hauri, E.H., Whitehouse, M.J., Price, A.A., Day, J.M., Shimizu, N. and Kelley, K.A., 2014. Volatile cycling of H_2O, CO_2, F, and Cl in the HIMU mantle: A new window provided by melt inclusions from oceanic hot spot lavas at Mangaia, Cook Islands. *Geochemistry, Geophysics, Geosystems*, *15*(11), 4445–4467. https://doi.org/10.1002/2014GC005473

Cartigny, P., Pineau, F., Aubaud, C., & Javoy, M. (2008). Towards a consistent mantle carbon flux estimate: Insights from volatile systematics (H_2O/Ce, δD, CO_2/Nb) in the North Atlantic mantle (14 N and 34 N). *Earth and Planetary Science Letters*, *265*(3–4), 672–685. https://doi.org/10.1016/j.epsl.2007.11.011

Danyushevsky, L. V., Della-Pasqua, F. N., & Sokolov, S. (2000). Re-equilibration of melt inclusions trapped by magnesian olivine phenocrysts from subduction-related magmas: petrological implications. *Contributions to Mineralogy and Petrology*, 138(1), 68–83. https://doi.org/10.1007/PL00007664

Danyushevsky, L. V., Leslie, R. A., Crawford, A. J., & Durance, P. (2004). Melt inclusions in primitive olivine phenocrysts: the role of localized reaction processes in the origin of anomalous compositions. *Journal of Petrology*, 45(12), 2531–2553. https://doi.org/10.1093/petrology/egh080

Danyushevsky, L. V., Perfit, M. R., Eggins, S. M., & Falloon, T. J. (2003). Crustal origin for coupled 'ultra-depleted' and 'plagioclase' signatures in MORB olivine-hosted melt inclusions: evidence from the Siqueiros Transform Fault, East Pacific Rise. *Contributions to Mineralogy and Petrology*, 144(5), 619–637. https://doi.org/10.1007/s00410-002-0420-3

Devey, C. W., Albarede, F., Cheminée, J. L., Michard, A., Mühe, R., & Stoffers, P. (1990). Active submarine volcanism on the Society hotspot swell (West Pacific): a geochemical study. *Journal of Geophysical Research: Solid Earth*, *95*(B4), 5049–5066. https://doi.org/10.1029/JB095iB04p05049

DeVitre, C. L., Allison, C. M., & Gazel, E. (2021). A high-precision CO_2 densimeter for Raman spectroscopy using a Fluid Density Calibration Apparatus. *Chemical Geology*, *584*, 120522. https://doi.org/10.1016/j.chemgeo.2021.120522

Dixon, J.E., Bindeman, I.N., Kingsley, R.H., Simons, K.K., Le Roux, P.J., Hajewski, T.R., Swart, P., Langmuir, C.H., Ryan, J.G., Walowski, K.J., & Wada, I. (2017). Light stable isotopic compositions of

enriched mantle sources: Resolving the dehydration paradox. *Geochemistry, Geophysics, Geosystems*, *18*(11), 3801–3839. https://doi.org/10.1002/2016GC006743

Dixon, J. E., & Clague, D. A. (2001). Volatiles in basaltic glasses from Loihi Seamount, Hawaii: Evidence for a relatively dry plume component. *Journal of Petrology*, *42*(3), 627–654. https://doi.org/10.1093/petrology/42.3.627

Dixon, J. E., Clague, D. A., Wallace, P., & Poreda, R. (1997). Volatiles in alkalic basalts form the North Arch Volcanic Field, Hawaii: extensive degassing of deep submarine-erupted alkalic series lavas. *Journal of Petrology*, 38(7), 911–939. https://doi.org/10.1093/petroj/38.7.911

Dixon, J. E., Leist, L., Langmuir, C., & Schilling, J. G. (2002). Recycled dehydrated lithosphere observed in plume-influenced mid-ocean-ridge basalt. *Nature*, *420*(6914), 385–389. https://doi.org/10.1038/nature01215

Farley, K. A., Natland, J. H., & Craig, H. (1992). Binary mixing of enriched and undegassed (primitive?) mantle components (He, Sr, Nd, Pb) in Samoan lavas. *Earth and Planetary Science Letters*, *111*(1), 183–199. https://doi.org/10.1016/0012-821X(92)90178-X

Ford, C. E., Russell, D. G., Craven, J. A., & Fisk, M. R. (1983). Olivine-liquid equilibria: temperature, pressure and composition dependence of the crystal/liquid cation partition coefficients for Mg, Fe^{2+}, Ca and Mn. *Journal of Petrology*, 24(3), 256–266. https://doi.org/10.1093/petrology/24.3.256

Fortin, M. A., Riddle, J., Desjardins-Langlais, Y., & Baker, D. R. (2015). The effect of water on the sulfur concentration at sulfide saturation (SCSS) in natural melts. *Geochimica et Cosmochimica Acta*, 160, 100–116. https://doi.org/10.1016/j.gca.2015.03.022

Fretzdorff, S., & Haase, K. M. (2002). Geochemistry and petrology of lavas from the submarine flanks of Réunion Island (western Indian Ocean): implications for magma genesis and the mantle source. *Mineralogy and Petrology*, 75, 153–184. https://doi.org/10.1007/s007100200022

Frey, F. A., Clague, D., Mahoney, J. J., & Sinton, J. M. (2000). Volcanism at the edge of the Hawaiian plume: petrogenesis of submarine alkalic lavas from the North Arch volcanic field. *Journal of Petrology*, 41(5), 667–691. https://doi.org/10.1093/petrology/41.5.667

Frezzotti, M. L. (2001). Silicate-melt inclusions in magmatic rocks: applications to petrology. *Lithos*, *55*(1–4), 273–299. https://doi.org/10.1016/S0024-4937(00)00048-7

Gaetani, G. A., & Grove, T. L. (1998). The influence of water on melting of mantle peridotite. *Contributions to Mineralogy and Petrology*, *131*, 323–346. https://doi.org/10.1007/s004100050396

Gaetani, G. A., O'Leary, J. A., Shimizu, N., Bucholz, C. E., & Newville, M. (2012). Rapid reequilibration of H_2O and oxygen fugacity in olivine-hosted melt inclusions. *Geology*, 40(10), 915–918. https://doi.org/10.1130/G32992.1

865 Ghiorso, M. S., & Gualda, G. A. (2015). An H_2O–CO_2 mixed fluid saturation model compatible with
866 rhyolite-MELTS. *Contributions to Mineralogy and Petrology*, 169, 1–30. https://doi.org/10.1007/s00410-
867 015-1141-8

868 Graham, D. W., & Michael, P. J. (2021). Predominantly recycled carbon in Earth's upper mantle revealed
869 by He-CO_2-Ba systematics in ultradepleted ocean ridge basalts. *Earth and Planetary Science Letters*, *554*,
870 116646. https://doi.org/10.1016/j.epsl.2020.116646

871 Gualda G.A.R., Ghiorso M.S., Lemons R.V., Carley T.L. (2012) Rhyolite-MELTS: A modified
872 calibration of MELTS optimized for silica-rich, fluid-bearing magmatic systems. *Journal of Petrology*,
873 *53*, 875–890. https://doi.org/10.1093/petrology/egr080

874 Hanyu, T., Yamamoto, J., Kimoto, K., Shimizu, K., & Ushikubo, T. (2020). Determination of total CO_2 in
875 melt inclusions with shrinkage bubbles. *Chemical Geology*, 557, 119855.
876 https://doi.org/10.1016/j.chemgeo.2020.119855

877 Hartley, M. E., Maclennan, J., Edmonds, M., & Thordarson, T. (2014). Reconstructing the deep CO_2
878 degassing behaviour of large basaltic fissure eruptions. *Earth and Planetary Science Letters*, 393, 120–
879 131. https://doi.org/10.1016/j.epsl.2014.02.031

880 Hartley, M. E., Neave, D. A., Maclennan, J., Edmonds, M., & Thordarson, T. (2015). Diffusive over-
881 hydration of olivine-hosted melt inclusions. *Earth and Planetary Science Letters*, 425, 168–178.
882 https://doi.org/10.1016/j.epsl.2015.06.008

883 Hauri, E. H. (1996). Major-element variability in the Hawaiian mantle plume. *Nature*, *382*(6590), 415–
884 419. https://doi.org/10.1038/382415a0

885 Hauri, E. H., & Hart, S. R. (1993). ReOs isotope systematics of HIMU and EMII oceanic island basalts
886 from the south Pacific Ocean. *Earth and Planetary Science Letters*, 114(2–3), 353–371.
887 https://doi.org/10.1016/0012-821X(93)90036-9

888 Hauri, E. (2002). SIMS analysis of volatiles in silicate glasses, 2: isotopes and abundances in Hawaiian
889 melt inclusions. *Chemical Geology*, *183*(1–4), 115–141. https://doi.org/10.1016/S0009-2541(01)00374-6

890 Hauri, E. H., Maclennan, J., McKenzie, D., Gronvold, K., Oskarsson, N., & Shimizu, N. (2018). CO_2
891 content beneath northern Iceland and the variability of mantle carbon. *Geology*, *46*(1), 55–58.
892 https://doi.org/10.1130/G39413.1

893 Hirschmann, M. M. (2006). Water, melting, and the deep Earth H_2O cycle. *Annu. Rev. Earth Planet.*
894 *Sci.*, *34*, 629–653. https://doi.org/10.1146/annurev.earth.34.031405.125211

895 Hirschmann, M. M. (2018). Comparative deep Earth volatile cycles: The case for C recycling from
896 exosphere/mantle fractionation of major (H_2O, C, N) volatiles and from H_2O/Ce, CO_2/Ba, and CO_2/Nb
897 exosphere ratios. *Earth and Planetary Science Letters*, *502*, 262–273.
898 https://doi.org/10.1016/j.epsl.2018.08.023

899 Hirth, G., & Kohlstedt, D. L. (1996). Water in the oceanic upper mantle: implications for rheology, melt
900 extraction and the evolution of the lithosphere. *Earth and Planetary Science Letters*, *144*(1-2), 93-108.
901 https://doi.org/10.1016/0012-821X(96)00154-9

Hirth, G., & Kohlstedf, D. (2003). Rheology of the upper mantle and the mantle wedge: A view from the experimentalists. *Geophysical Monograph-American Geophysical Union*, *138*, 83–106. https://doi.org/10.1029/138GM06

Hofmann, A. W., Jochum, K. P., Seufert, M., & White, W. M. (1986). Nb and Pb in oceanic basalts: new constraints on mantle evolution. *Earth and Planetary Science Letters*, 79(1–2), 33–45. https://doi.org/10.1016/0012-821X(86)90038-5

Iacovino, K., Matthews, S., Wieser, P. E., Moore, G. M., & Bégué, F. (2021). VESIcal Part I: An open-source thermodynamic model engine for mixed volatile (H_2O-CO_2) solubility in silicate melts. *Earth and Space Science*, 8(11), e2020EA001584. https://doi.org/10.1029/2020EA001584

Jackson, M. G., & Hart, S. R. (2006). Strontium isotopes in melt inclusions from Samoan basalts: Implications for heterogeneity in the Samoan plume. *Earth and Planetary Science Letters*, 245(1–2), 260–277. https://doi.org/10.1016/j.epsl.2006.02.040

Jackson, M. G., & Macdonald, F. A. (2022). Hemispheric geochemical dichotomy of the mantle is a legacy of austral supercontinent assembly and onset of deep continental crust subduction. *AGU Advances*, 3(6), e2022AV000664. https://doi.org/10.1029/2022AV000664

Jackson, M. G., Kurz, M. D., Hart, S. R., & Workman, R. K. (2007). New Samoan lavas from Ofu Island reveal a hemispherically heterogeneous high $^3He/^4He$ mantle. *Earth and Planetary Science Letters*, *264*(3–4), 360–374. https://doi.org/10.1016/j.epsl.2007.09.023

Jackson, M.G., Koga, K.T., Price, A., Konter, J.G., Koppers, A.A., Finlayson, V.A., Konrad, K., Hauri, E.H., Kylander-Clark, A., Kelley, K.A., & Kendrick, M.A. (2015). Deeply dredged submarine HIMU glasses from the Tuvalu Islands, Polynesia: Implications for volatile budgets of recycled oceanic crust. *Geochemistry, Geophysics, Geosystems*, *16*(9), 3210–3234. https://doi.org/10.1002/2015GC005966

Jackson, M. G., Hart, S. R., Konter, J. G., Kurz, M. D., Blusztajn, J., & Farley, K. A. (2014). Helium and lead isotopes reveal the geochemical geometry of the Samoan plume. *Nature*, *514*(7522), 355–358. https://doi.org/10.1038/nature13794

Kendrick, M. A., Arculus, R., Burnard, P., & Honda, M. (2013). Quantifying brine assimilation by submarine magmas: Examples from the Galápagos Spreading Centre and Lau Basin. *Geochimica et Cosmochimica Acta*, 123, 150–165. https://doi.org/10.1016/j.gca.2013.09.012

Kendrick, M. A., Jackson, M. G., Kent, A. J., Hauri, E. H., Wallace, P. J., & Woodhead, J. (2014). Contrasting behaviours of CO_2, S, H_2O and halogens (F, Cl, Br, and I) in enriched-mantle melts from Pitcairn and Society seamounts. *Chemical Geology*, 370, 69–81. https://doi.org/10.1016/j.chemgeo.2014.01.019

Kendrick, M. A., Hémond, C., Kamenetsky, V. S., Danyushevsky, L., Devey, C. W., Rodemann, T., Jackson, M. G., & Perfit, M. R. (2017). Seawater cycled throughout Earth's mantle in partially serpentinized lithosphere. *Nature Geoscience*, 10(3), 222–228. https://doi.org/10.1038/ngeo2902

Kendrick, M. A., Jackson, M. G., Hauri, E. H., & Phillips, D. (2015). The halogen (F, Cl, Br, I) and H_2O systematics of Samoan lavas: Assimilated-seawater, EM2 and high-$^3He/^4He$ components. *Earth and Planetary Science Letters*, 410, 197–209. https://doi.org/10.1016/j.epsl.2014.11.026

Kent, A. J. R., Clague, D. A., Honda, M., Stolper, E. M., Hutcheon, I. D., & Norman, M. D. (1999a). Widespread assimilation of a seawater-derived component at Loihi Seamount, Hawaii. *Geochimica et Cosmochimica Acta*, 63(18), 2749–2761. https://doi.org/10.1016/S0016-7037(99)00215-X

Kent, A. J. R., Norman, M. D., Hutcheon, I. D., & Stolper, E. M. (1999b). Assimilation of seawater-derived components in an oceanic volcano: evidence from matrix glasses and glass inclusions from Loihi seamount, Hawaii. *Chemical Geology*, *156*(1–4), 299–319. https://doi.org/10.1016/S0009-2541(98)00188-0

Kent, A. J. R., Peate, D. W., Newman, S., Stolper, E. M., & Pearce, J. A. (2002). Chlorine in submarine glasses from the Lau Basin: seawater contamination and constraints on the composition of slab-derived fluids. *Earth and Planetary Science Letters*, 202(2), 361–377. https://doi.org/10.1016/S0012-821X(02)00786-0

Koleszar, A. M., Saal, A. E., Hauri, E. H., Nagle, A. N., Liang, Y., & Kurz, M. D. (2009). The volatile contents of the Galapagos plume; evidence for H_2O and F open system behavior in melt inclusions. *Earth and Planetary Science Letters*, 287(3–4), 442–452. https://doi.org/10.1016/j.epsl.2009.08.029

Labidi, J., Cartigny, P., & Jackson, M. G. (2015). Multiple sulfur isotope composition of oxidized Samoan melts and the implications of a sulfur isotope 'mantle array' in chemical geodynamics. *Earth and Planetary Science Letters*, *417*, 28–39. https://doi.org/10.1016/j.epsl.2015.02.004

Lassiter, J. C., Hauri, E. H., Nikogosian, I. K., & Barsczus, H. G. (2002). Chlorine–potassium variations in melt inclusions from Raivavae and Rapa, Austral Islands: constraints on chlorine recycling in the mantle and evidence for brine-induced melting of oceanic crust. *Earth and Planetary Science Letters*, *202*(3–4), 525–540. https://doi.org/10.1016/S0012-821X(02)00826-9

Le Roux, P. J., Shirey, S. B., Hauri, E. H., Perfit, M. R., & Bender, J. F. (2006). The effects of variable sources, processes and contaminants on the composition of northern EPR MORB (8–10°N and 12–14°N): Evidence from volatiles (H_2O, CO_2, S) and halogens (F, Cl). *Earth and Planetary Science Letters*, *251*(3–4), 209–231. https://doi.org/10.1016/j.epsl.2006.09.012

Le Voyer, M., Kelley, K. A., Cottrell, E., & Hauri, E. H. (2017). Heterogeneity in mantle carbon content from CO_2-undersaturated basalts. *Nature Communications*, 8(1), 14062. https://doi.org/10.1038/ncomms14062

Le Voyer, M., Hauri, E.H., Cottrell, E., Kelley, K.A., Salters, V.J., Langmuir, C.H., Hilton, D.R., Barry, P.H. & Füri, E. (2019). Carbon fluxes and primary magma CO_2 contents along the global mid-ocean ridge system. *Geochemistry, Geophysics, Geosystems*, *20*(3), 1387–1424. https://doi.org/10.1029/2018GC007630

Loewen, M. W., Graham, D. W., Bindeman, I. N., Lupton, J. E., & Garcia, M. O. (2019). Hydrogen isotopes in high $^{3}He/^{4}He$ submarine basalts: Primordial vs. recycled water and the veil of mantle enrichment. *Earth and Planetary Science Letters*, *508*, 62–73. https://doi.org/10.1016/j.epsl.2018.12.012

Machida, S., Hirano, N., Sumino, H., Hirata, T., Yoneda, S. & Kato, Y. (2015). Petit-spot geology reveals melts in upper-most asthenosphere dragged by lithosphere. *Earth and Planetary Science Letters*, 426, 267–279. https://doi.org/10.1016/j.epsl.2015.06.018

Matthews, S., Shorttle, O., Maclennan, J., & Rudge, J. F. (2021). The global melt inclusion C/Ba array: Mantle variability, melting process, or degassing?. *Geochimica et Cosmochimica Acta*, *293*, 525–543. https://doi.org/10.1016/j.gca.2020.09.030

McDonough, W. F., & Sun, S. S. (1995). The composition of the Earth. *Chemical Geology*, 120, 223–253. https://doi.org/10.1016/0009-2541(94)00140-4

Métrich, N., Zanon, V., Créon, L., Hildenbrand, A., Moreira, M., & Marques, F. O. (2014). Is the 'Azores hotspot'a wetspot? Insights from the geochemistry of fluid and melt inclusions in olivine of Pico basalts. *Journal of Petrology*, *55*(2), 377–393. https://doi.org/10.1093/petrology/egt071

Miller, W. G., Maclennan, J., Shorttle, O., Gaetani, G. A., Le Roux, V., & Klein, F. (2019). Estimating the carbon content of the deep mantle with Icelandic melt inclusions. *Earth and Planetary Science Letters*, *523*, 115699. https://doi.org/10.1016/j.epsl.2019.07.002

Michael, P. (1995). Regionally distinctive sources of depleted MORB: Evidence from trace elements and H_2O. *Earth and Planetary Science Letters*, *131*(3-4), 301–320. https://doi.org/10.1016/0012-821X(95)00023-6

Michael, P. J., & Graham, D. W. (2015). The behavior and concentration of CO_2 in the suboceanic mantle: Inferences from undegassed ocean ridge and ocean island basalts. *Lithos*, *236*, 338–351. https://doi.org/10.1016/j.lithos.2015.08.020

Moore, L.R., Gazel, E., Tuohy, R., Lloyd, A.S., Esposito, R., Steele-MacInnis, M., Hauri, E.H., Wallace, P.J., Plank, T. & Bodnar, R.J. (2015). Bubbles matter: An assessment of the contribution of vapor bubbles to melt inclusion volatile budgets. *American Mineralogist*, *100*(4), 806–823. https://doi.org/10.2138/am-2015-5036

Portnyagin, M., Almeev, R., Matveev, S., & Holtz, F. (2008). Experimental evidence for rapid water exchange between melt inclusions in olivine and host magma. *Earth and Planetary Science Letters*, *272*(3–4), 541–552. https://doi.org/10.1016/j.epsl.2008.05.020

Portnyagin, M., Hoernle, K., Plechov, P., Mironov, N., & Khubunaya, S. (2007). Constraints on mantle melting and composition and nature of slab components in volcanic arcs from volatiles (H_2O, S, Cl, F) and trace elements in melt inclusions from the Kamchatka Arc. *Earth and Planetary Science Letters*, *255*(1-2), 53–69. https://doi.org/10.1016/j.epsl.2006.12.005

Reinhard, A.A., Jackson, M.G., Koornneef, J.M., Rose-Koga, E.F., Blusztajn, J., Konter, J.G., Koga, K.T., Wallace, P.J. & Harvey, J. (2018). Sr and Nd isotopic compositions of individual olivine-hosted melt inclusions from Hawai'i and Samoa: Implications for the origin of isotopic heterogeneity in melt

1009 inclusions from OIB lavas. *Chemical Geology*, *495*, 36–49.
1010 https://doi.org/10.1016/j.chemgeo.2018.07.034

1011 Roeder, P.L., & Emslie, R. (1970). Olivine-liquid equilibrium. *Contributions to Mineralogy and*
1012 *Petrology*, 29(4), 275–289. https://doi.org/10.1007/BF00371276

1013 Rose-Koga, E.F., Koga, K.T., Moreira, M., Vlastélic, I., Jackson, M.G., Whitehouse, M.J., Shimizu, N.,
1014 & Habib, N. (2017). Geochemical systematics of Pb isotopes, fluorine, and sulfur in melt inclusions from
1015 São Miguel, Azores. *Chemical Geology*, *458*, 22–37. https://doi.org/10.1016/j.chemgeo.2017.03.024

1016 Rose-Koga, E.F., Koga, K.T., Schiano, P., Le Voyer, M., Shimizu, N., Whitehouse, M.J., Clocchiatti, R.,
1017 2012. Mantle source heterogeneity for South Tyrrhenian magmas revealed by Pb isotopes and halogen
1018 contents of olivine-hosted melt inclusions. *Chemical Geology*, 334, 266–279.
1019 https://doi.org/10.1016/j.chemgeo.2012.10.033

1020 Rowe, M. C., & Lassiter, J. C. (2009). Chlorine enrichment in central Rio Grande Rift basaltic melt
1021 inclusions: Evidence for subduction modification of the lithospheric mantle. *Geology*, 37(5), 439–442.
1022 https://doi.org/10.1130/G25530A.1

1023 Ryan, W. B. F., Carbotte, S. M., Coplan, J. O., O'Hara, S., Melkonian, A., Arko, R., Weissel, R. A.,
1024 Ferrini, V., Goodwillie, A., Nitsche, F., Bonczkowski, J., & Zemsky, R. (2009). Global Multi-Resolution
1025 Topography synthesis. *Geochemistry, Geophysics, Geosystems*, 10, Q03014.
1026 https://doi.org/10.1029/2008GC002332

1027 Saal, A. E., Hauri, E. H., Langmuir, C. H., & Perfit, M. R. (2002). Vapour undersaturation in primitive
1028 mid-ocean-ridge basalt and the volatile content of Earth's upper mantle. *Nature*, 419(6906), 451–455.
1029 https://doi.org/10.1038/nature01073

1030 Shimizu, K., Saal, A. E., Hauri, E. H., Sinton, J. M., Janney, P. E., Geshi, N., & Hékinian, R. (2023).
1031 High-C content and CO_2/Ba ratio of the Earth's enriched upper mantle. *Geochimica et Cosmochimica*
1032 *Acta*. https://doi.org/10.1016/j.gca.2022.10.023

1033 Shimizu, K., Saal, A.E., Myers, C.E., Nagle, A.N., Hauri, E.H., Forsyth, D.W., Kamenetsky, V.S., & Niu,
1034 Y. (2016). Two-component mantle melting-mixing model for the generation of mid-ocean ridge basalts:
1035 Implications for the volatile content of the Pacific upper mantle. *Geochimica et Cosmochimica Acta*, *176*,
1036 44–80. https://doi.org/10.1016/j.gca.2015.10.033

1037 Sims, K. W. W., Hart, S.R., Reagan, M.K., Blusztajn, J., Staudigel, H., Sohn, R.A., Layne, G.D., Ball,
1038 L.A., & Andrews, J. (2008). 238U-230Th-226Ra-210Pb-210Po, 232Th-228Ra, and 235U-231Pa
1039 constraints on the ages and petrogenesis of Vailulu'u and Malumalu Lavas, Samoa. *Geochemistry,*
1040 *Geophysics, Geosystems*, 9, Q04003. https://doi.org/10.1029/2007GC001651.

1041 Smythe, D. J., Wood, B. J., & Kiseeva, E. S. (2017). The S content of silicate melts at sulfide saturation:
1042 new experiments and a model incorporating the effects of sulfide composition. *American Mineralogist*,
1043 102(4), 795–803. https://doi.org/10.2138/am-2017-5800CCBY

1044 Staudigel, H., Zindler, A., Hart, S. R., Leslie, T., Chen, C. Y., & Clague, D. (1984). The isotope
1045 systematics of a juvenile intraplate volcano: Pb, Nd, and Sr isotope ratios of basalts from Loihi Seamount,
1046 Hawaii. *Earth and Planetary Science Letters*, 69(1), 13–29. https://doi.org/10.1016/0012-
1047 821X(84)90071-2

1048 Sun, C., & Dasgupta, R. (2020). Thermobarometry of CO_2-rich, silica-undersaturated melts constrains
1049 cratonic lithosphere thinning through time in areas of kimberlitic magmatism. *Earth and Planetary*
1050 *Science Letters*, 550, 116549. https://doi.org/10.1016/j.epsl.2020.116549

1051 Taracsák, Z., Hartley, M. E., Burgess, R., Edmonds, M., Iddon, F., & Longpré, M. A. (2019). High fluxes
1052 of deep volatiles from ocean island volcanoes: Insights from El Hierro, Canary Islands. *Geochimica et*
1053 *Cosmochimica Acta*, *258*, 19–36. https://doi.org/10.1016/j.gca.2019.05.020

1054 Wallace, P. J. (2002). Volatiles in submarine basaltic glasses from the Northern Kerguelen Plateau (ODP
1055 Site 1140): Implications for source region compositions, magmatic processes, and plateau subsidence.
1056 *Journal of Petrology*, *43*(7), 1311–1326. https://doi.org/10.1093/petrology/43.7.1311

1057 Wanless, V. D., & Shaw, A. M. (2012). Lower crustal crystallization and melt evolution at mid-ocean
1058 ridges. *Nature Geoscience*, 5(9), 651–655. https://doi.org/10.1038/ngeo1552

1059 Wanless, V. D., Behn, M. D., Shaw, A. M., & Plank, T. (2014). Variations in melting dynamics and
1060 mantle compositions along the Eastern Volcanic Zone of the Gakkel Ridge: insights from olivine-hosted
1061 melt inclusions. *Contributions to Mineralogy and Petrology*, 167, 1–22. https://doi.org/10.1007/s00410-
1062 014-1005-7

1063 Wanless, V. D., Shaw, A. M., Behn, M. D., Soule, S. A., Escartín, J., & Hamelin, C. (2015). Magmatic
1064 plumbing at Lucky Strike volcano based on olivine-hosted melt inclusion compositions. *Geochemistry,*
1065 *Geophysics, Geosystems*, 16(1), 126–147. https://doi.org/10.1002/2014GC005517

1066 White, W. M., & Duncan, R. A. (1996). Geochemistry and geochronology of the Society Islands: New
1067 evidence for deep mantle recycling. *Geophysical Monograph-American Geophysical Union*, *95*, 183–206.

1068 White, W. M., & Hofmann, A. W. (1982). Sr and Nd isotope geochemistry of oceanic basalts and mantle
1069 evolution. *Nature*, *296*(5860), 821–825. https://doi.org/10.1038/296821a0

1070 Wieser, P. E., Iacovino, K., Matthews, S., Moore, G., & Allison, C. M. (2022). VESIcal: 2. A Critical
1071 Approach to Volatile Solubility Modeling Using an Open-Source Python3 Engine. *Earth and Space*
1072 *Science*, 9(2), e2021EA001932. https://doi.org/10.1029/2021EA001932

1073 Workman, R.K., Hart, S.R., Jackson, M., Regelous, M., Farley, K.A., Blusztajn, J., Kurz, M. & Staudigel,
1074 H. (2004). Recycled metasomatized lithosphere as the origin of the Enriched Mantle II (EM2) end-
1075 member: Evidence from the Samoan Volcanic Chain. *Geochemistry, Geophysics, Geosystems*, 5(4).
1076 https://doi.org/10.1029/2003GC000623

1077 Workman, R. K., Hauri, E., Hart, S. R., Wang, J., & Blusztajn, J. (2006). Volatile and trace elements in
1078 basaltic glasses from Samoa: Implications for water distribution in the mantle. *Earth and Planetary*
1079 *Science Letters*, *241*(3–4), 932–951. https://doi.org/10.1016/j.epsl.2005.10.028

Woodhead, J. D., & Devey, C. W. (1993). Geochemistry of the Pitcairn seamounts, I: source character and temporal trends. *Earth and Planetary Science Letters*, *116*(1–4), 81–99. https://doi.org/10.1016/0012-821X(93)90046-C

FIGURES

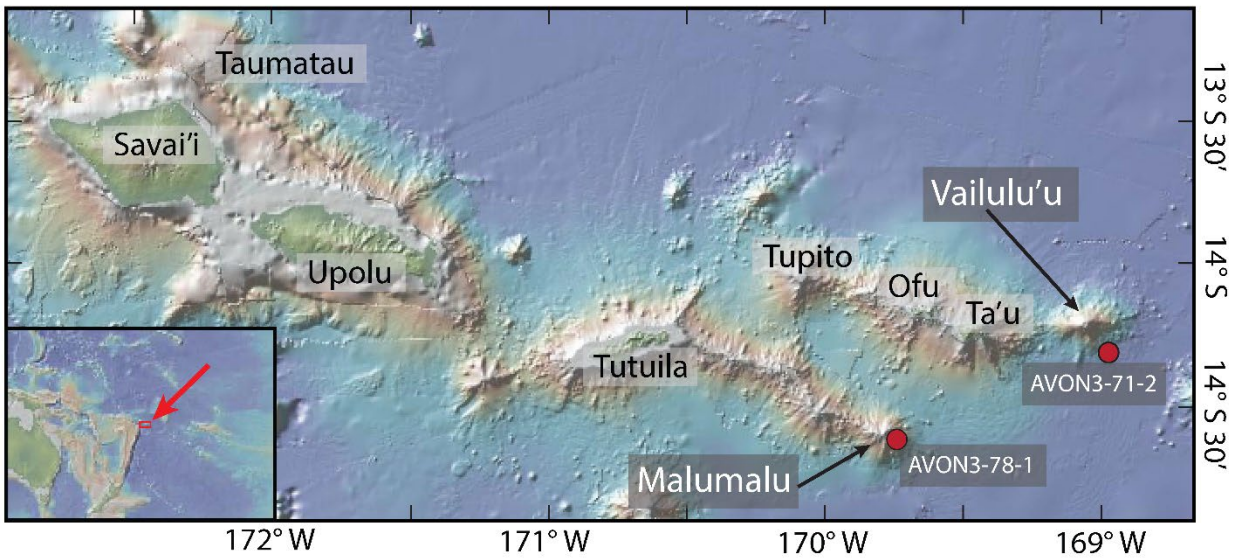

Figure 1. Map of the Samoan Islands. Red dots indicate the location of AVON3 cruise dredge sites 71 and 78, from the flanks of Vailulu'u and Malumalu, respectively. Map created using GeoMapApp (www.geomapapp.org).

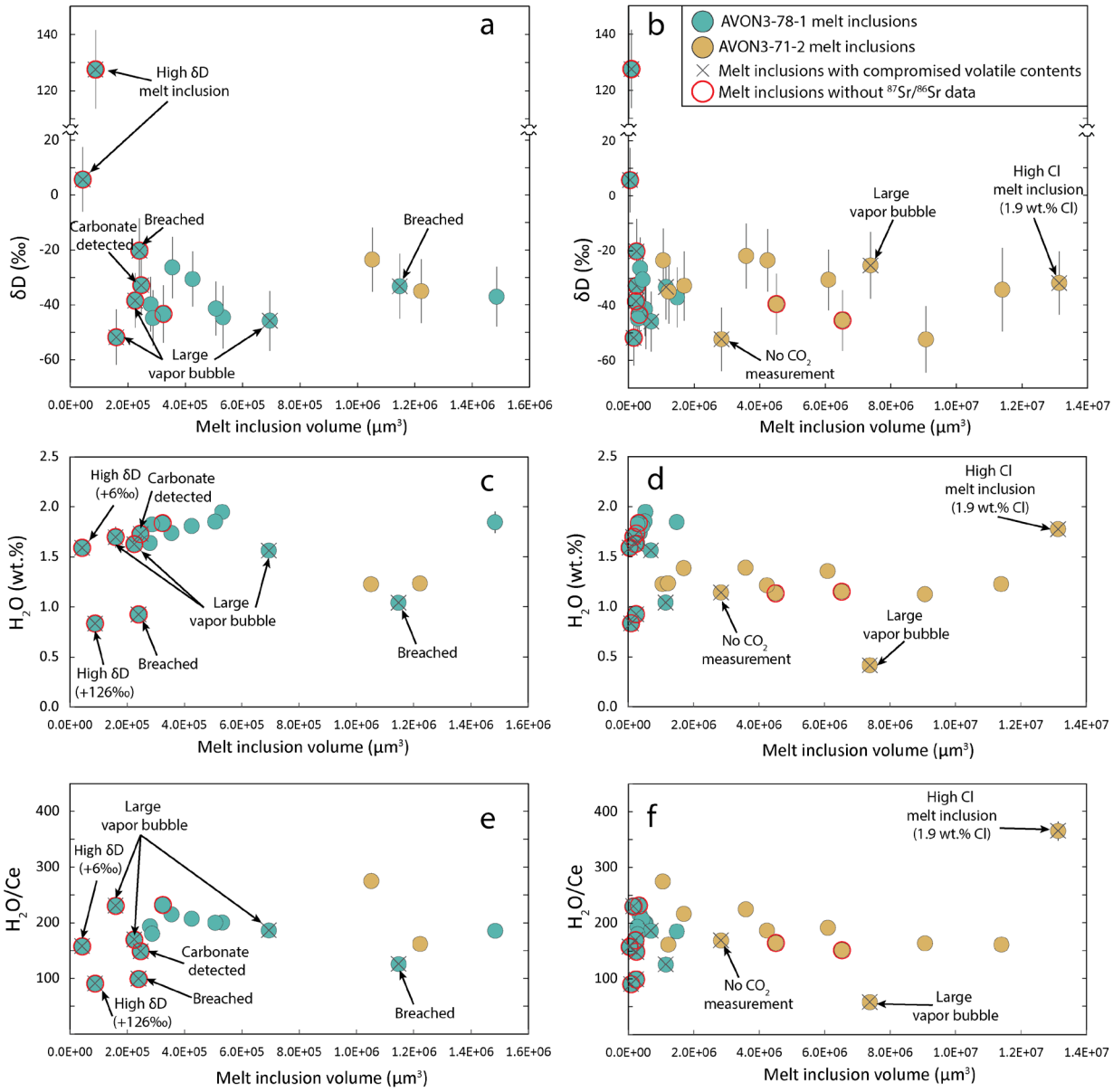

Figure 2. (a–b) δD (‰), **(c–d)** H_2O (wt.%), and **(e–f)** H_2O/Ce versus melt inclusion volume (µm^3). Left-hand side panels focus (zoom in) on the Malumalu melt inclusions and right-hand side panels (zoom out) to show the Vailulu'u melt inclusions. In panel (a) δD errors represent the 2σ in run measurement precision of each analysis, which is generally slightly lower than the reproducibility of the secondary standard ALV1833-1 (i.e., ±16‰, 2SD; see Table S2). Melt inclusion H_2O compositions are corrected for olivine addition/subtraction to be in equilibrium with the host olivine (olivine correction is as in Section 2 of the main text). Measurement errors for H_2O, and reproducibility of H_2O analyses on ALV1833-1, are smaller than the data symbol (see Table S2). As discussed in Section 3 of the text, we infer that the volatile contents of eleven melt inclusions shown in this figure have been compromised in one of several ways—hydrogen diffusion loss (and resultant elevated δD), breaching, large vapor bubbles, extremely high Cl concentrations, presence of carbonate, and/or missing Raman-based CO_2 data—and are marked with an "x" symbol. With the exception of the high Cl melt inclusion (which is individually identified in

figures throughout the paper), the compromised melt inclusions are not shown in subsequent volatile element figures.

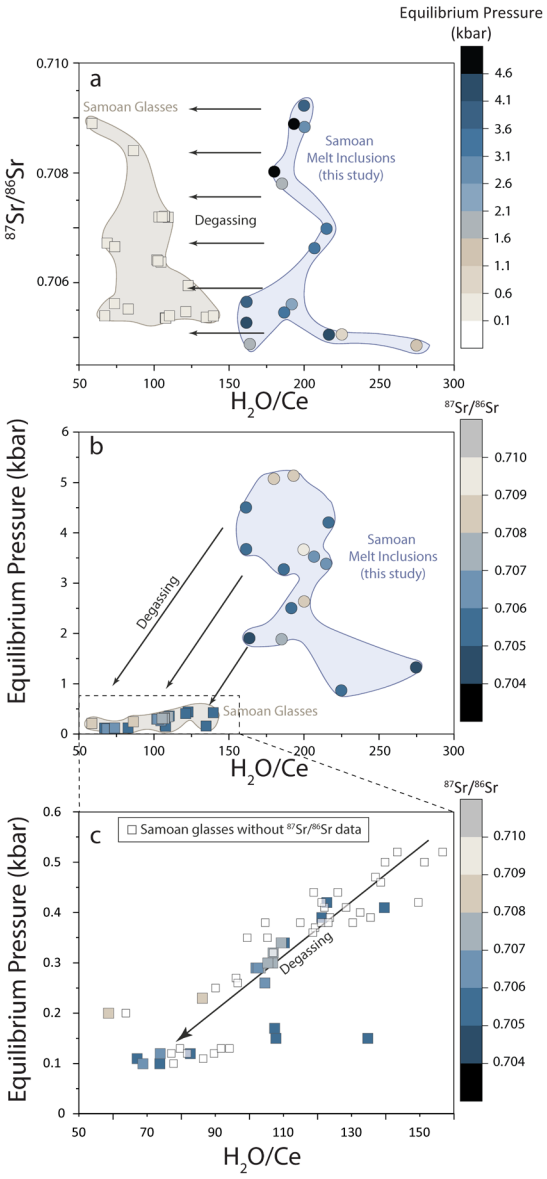

Figure 3. $^{87}Sr/^{86}Sr$, H_2O/Ce, and equilibrium pressure for submarine pillow glasses from Malumalu and Vailulu'u seamounts are compared with melt inclusions from Malumalu sample AVON3-78-1 and Vailulu'u sample AVON3-71-2. (a) $^{87}Sr/^{86}Sr$ versus H_2O/Ce for Samoan melt inclusions and glasses with the color bar representing equilibrium pressure (kbar). The pillow glass data show separation in H_2O/Ce from the melt inclusion data, even though both datasets span a similar range in $^{87}Sr/^{86}Sr$. Circles represent melt inclusions and squares represent Samoan pillow glasses from Workman et al. (2006). Melt inclusions in this figure do not include any volatile-compromised melt inclusions (as shown in Figure 2). The equilibrium pressure of pillow glasses and melt inclusions was calculated using VESIcal's MagmaSat model (Iacovino et al., 2021; Wieser et al., 2022) assuming oxygen fugacity (QFM) and temperature (1200°C). Samoan pillow glass data are from Workman et al. (2006), except major elements used to calculate equilibrium pressure for AVON3-71-2 and AVON3-78-1 (which are from Kendrick et al.,

2015). (b) Equilibrium pressure versus H_2O/Ce for Samoan melt inclusions and pillow glasses with the color bar representing $^{87}Sr/^{86}Sr$. (c) Expanded view of panel b that shows equilibrium pressure versus H_2O/Ce for Samoan pillow glasses only. Smaller square data points with black outlines are pillow glasses lacking $^{87}Sr/^{86}Sr$ data. Only samples with CO_2-H_2O saturation pressures ≥0.1 kbar are shown (just one Samoan glass with $^{87}Sr/^{86}Sr$ data has a saturation pressure <0.1 kbar, sample AVON3-68-03 Rpt, so its removal does not significantly impact the dataset).

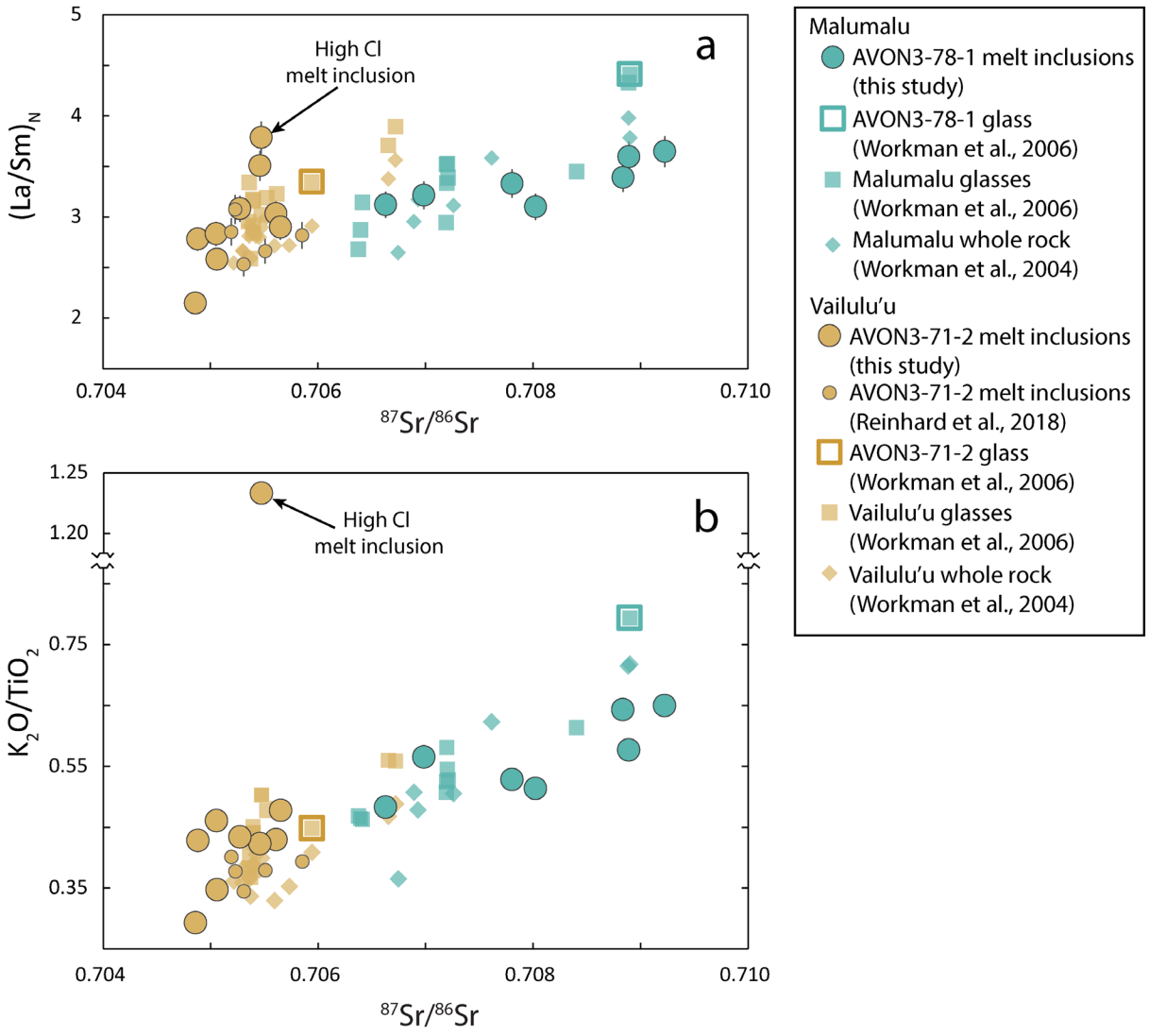

Figure 4. Incompatible trace element ratios versus $^{87}Sr/^{86}Sr$ are shown for Samoan pillow glasses from Malumalu and Vailulu'u seamounts and new melt inclusion data from Malumalu sample AVON3-78-1 and Vailulu'u sample AVON3-71-2. The melt inclusions have incompatible trace element ratios and $^{87}Sr/^{86}Sr$ compositions that fall within the range identified in Samoan pillow glasses, indicating that the Samoan melt inclusions sample melts represented by the pillow glass dataset. (a) $(La/Sm)_N$ versus $^{87}Sr/^{86}Sr$, where N signifies normalization to primitive mantle (McDonough & Sun, 1995). (b) K_2O/TiO_2

versus $^{87}Sr/^{86}Sr$. Data for Samoan pillow glasses are from Workman et al. (2006) and Kendrick et al. (2015). Error bars for La/Sm (4.2%) are shown for the melt inclusions and are calculated as ((La error)^2+(Sm error)^2)$^{0.5}$, where the 2RSD of the secondary standard BCR-2 is used for La error (1.9%) and Sm error (3.8%) (see Table S2). Error bars on K_2O/TiO_2 are smaller than the data symbols. Melt inclusions that are compromised with respect to their volatile contents are not shown, except for the high Cl melt inclusion.

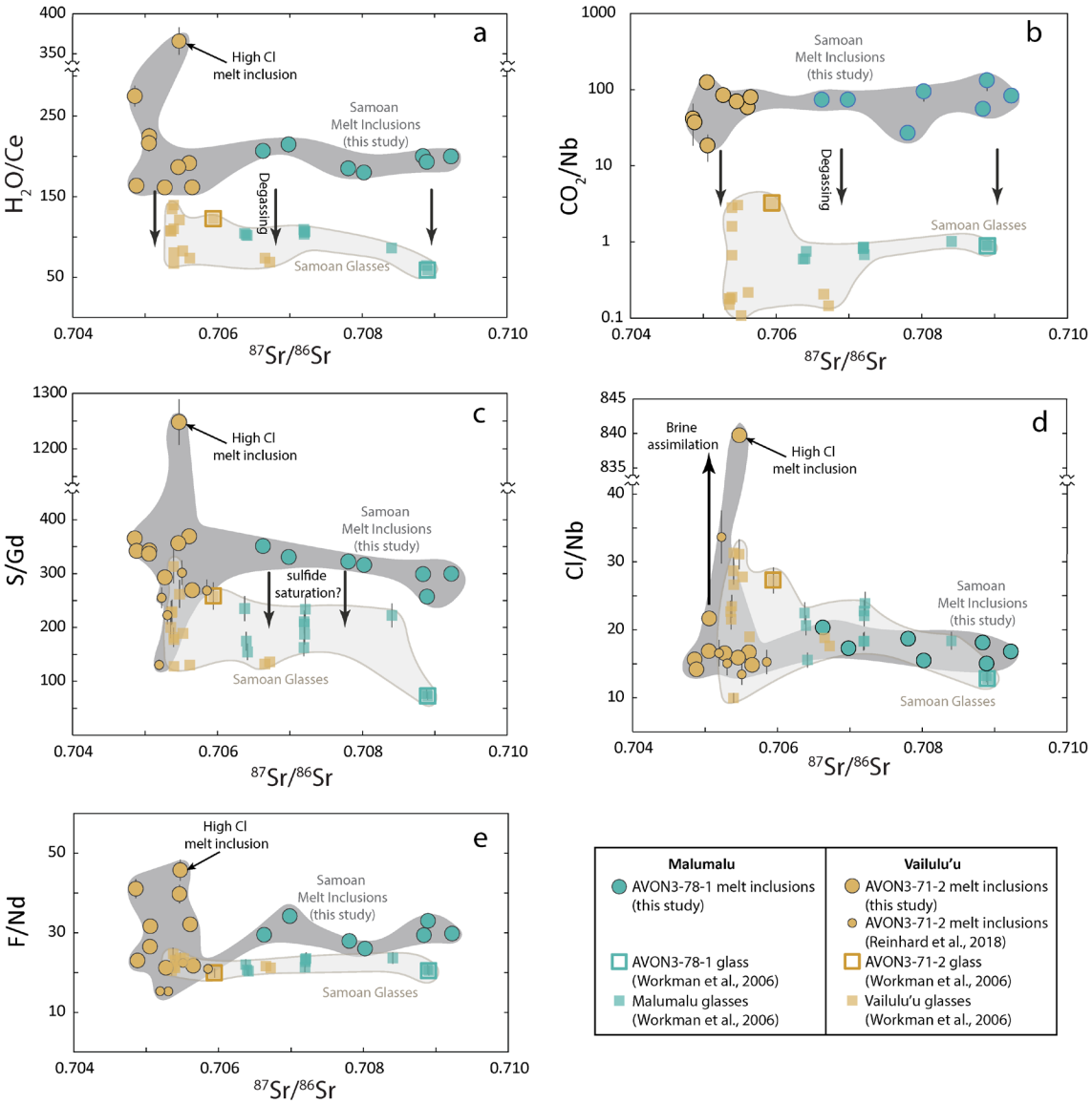

Figure 5. Element ratios (volatile/incompatible trace element) are plotted against $^{87}Sr/^{86}Sr$ for Samoan pillow glasses from Malumalu and Vailulu'u seamounts and the new melt inclusion data from Malumalu sample AVON3-78-1 and Vailulu'u sample AVON3-71-2. See Supplementary Text section S1.6 for a discussion on the calculation of the errors associated with the element ratios presented here; the error bars for the $^{87}Sr/^{86}Sr$ of Samoan glasses and melt inclusions are smaller than the symbol size. Melt inclusions that are compromised with respect to their volatile contents (as shown in Figure 2) are not

shown. Only samples with CO_2-H_2O saturation pressures ≥0.1 kbar are shown (just one Samoan glass with $^{87}Sr/^{86}Sr$ data has a saturation pressure <0.1 kbar, sample AVON3-68-03 Rpt, so its removal does not significantly impact the dataset).

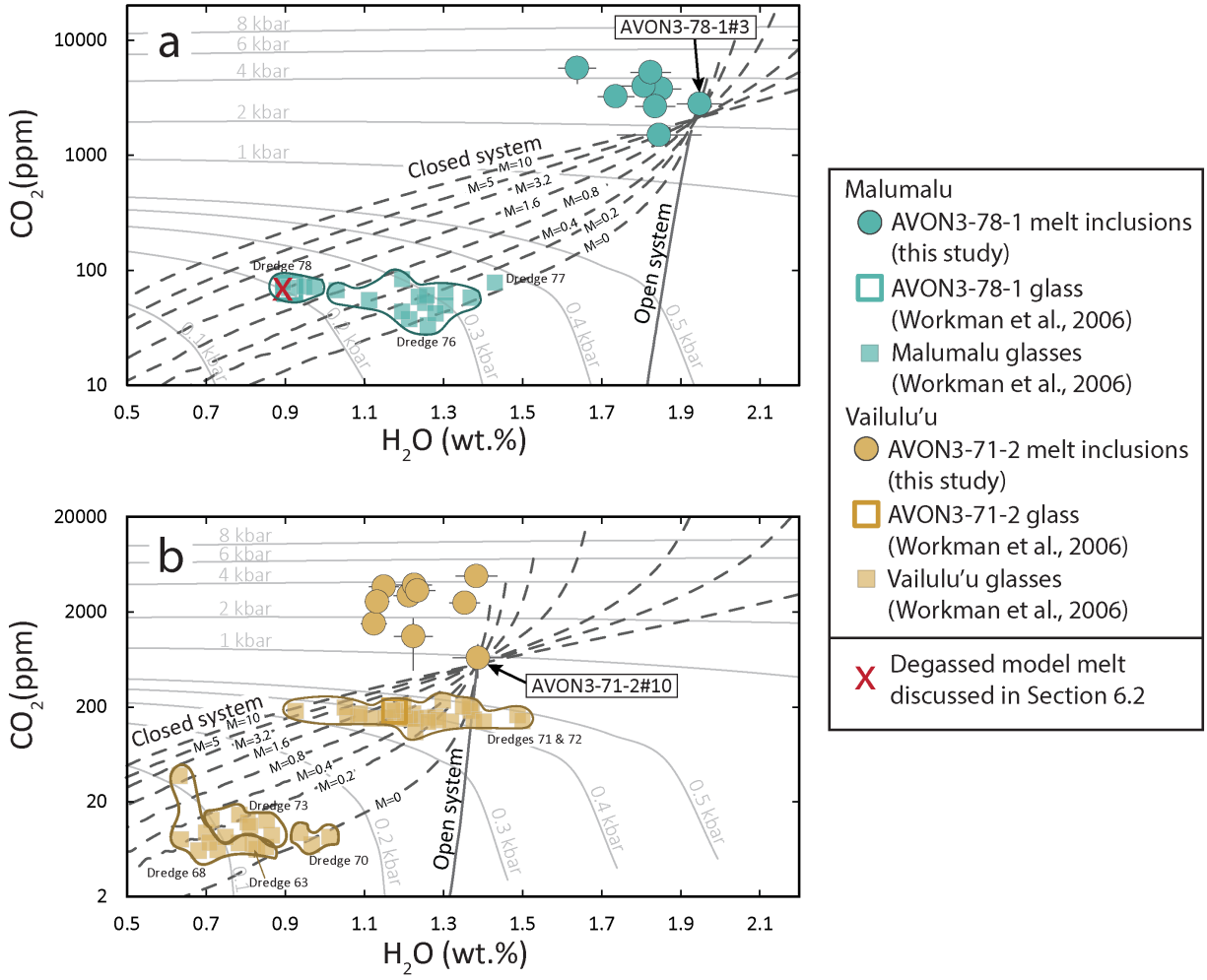

Figure 6. CO_2 versus H_2O for (a) melt inclusions from Malumalu sample AVON3-78-1 and all glasses from Malumalu seamount and (b) melt inclusions from Vailulu'u sample AVON3-71-2 and all glasses from Vailulu'u seamount. Melt inclusion data are from this study and Samoan glass data are from Workman et al. (2006) and the data are shown in fields separated by the dredge number (which is provided next to the relevant field). Isobars are calculated using MagmaSat for an average melt inclusion composition of each sample at 1200°C. Closed system degassing curves are calculated with varying values for M (where "M" represents mass fraction of equilibrium fluid in the magma; e.g., M=1.6 means there was 1.6 wt.% of fluid in the magma before degassing). Degassing trends assume an oxygen fugacity (QFM) and temperature (1200°C) and are calculated in rhyolite-MELTS v1.2 using H_2O and CO_2 compositions that match the highest H_2O melt inclusions in the respective panels (i.e., Malumalu melt inclusion AVON3-78-

1#3 in the upper panel, and Vailulu'u melt inclusion AVON3-71-2#10 in the lower panel); other compositions used in the degassing calculation are in Table S9. Melt inclusion CO_2 and H_2O concentrations shown are values that have been corrected to be in equilibrium with the host olivine. Volatile-compromised melt inclusions (as shown in Figure 2) are not included in this figure.

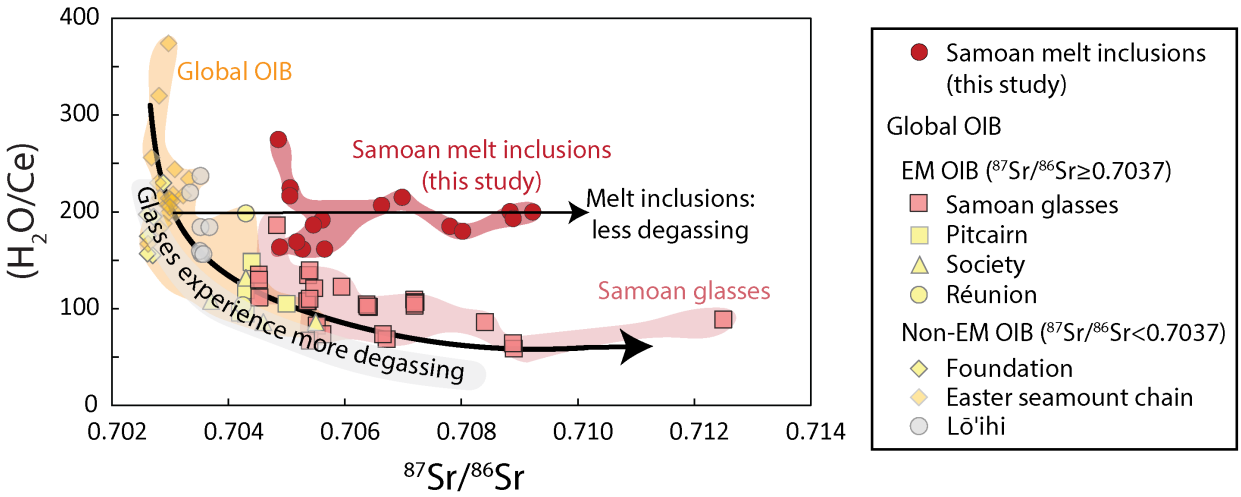

Figure 7. Samoan melt inclusions and pillow glasses compared to a global dataset of submarine OIB glasses. Samoan melt inclusions—protected from the extensive degassing experienced by Samoan glasses—have higher H_2O/Ce than Samoan pillow glasses, and thus fall off of the global submarine OIB pillow glass trend that shows decreasing H_2O/Ce with increasing $^{87}Sr/^{86}Sr$. Only OIB glasses with $^{87}Sr/^{86}Sr$ (to establish the level of source enrichment) and MgO > 4.5 wt.% (to minimize the impact of fractional crystallization) are shown. Sources of data (see Table S11): Pitcairn (Kendrick et al., 2014; Woodhead & Devey, 1993), Society (Devey et al., 1990; Kendrick et al., 2014), Réunion (Kendrick et al., 2017; Fretzdorf & Haase, 2002), Foundation (Kendrick et al., 2017), Easter seamount chain (Dixon et al., 2002), Lō'ihi (Dixon & Clague, 2001; Staudigel et al., 1984). Samples from Pitcairn, Society, Réunion, and Foundation can be found in a data compilation by Kendrick et al. (2017). Samples marked as having experienced assimilation of seawater Cl in Kendrick et al. (2017) are excluded. However, unlike Dixon et al. (2002), we do not use H_2O/Ce as a filter for assimilation. Samoan pillow glasses include submarine glasses characterized for $^{87}Sr/^{86}Sr$ from Vailulu'u, Malumalu, Tupito (formerly known as Muli), Taumatau, and Ta'u (Kendrick et al., 2015; Workman et al., 2006). Volatile-compromised melt inclusions (as shown in Figure 2) are not shown. Melt inclusions from other OIB localities are not shown because there are no other OIB melt inclusions characterized for both $^{87}Sr/^{86}Sr$ and H_2O/Ce. Only samples with CO_2-H_2O saturation pressures ≥0.1 kbar are shown (just one Samoan glass with $^{87}Sr/^{86}Sr$ data has a saturation pressure <0.1 kbar, sample AVON3-68-03 Rpt, so its removal does not significantly impact the dataset).

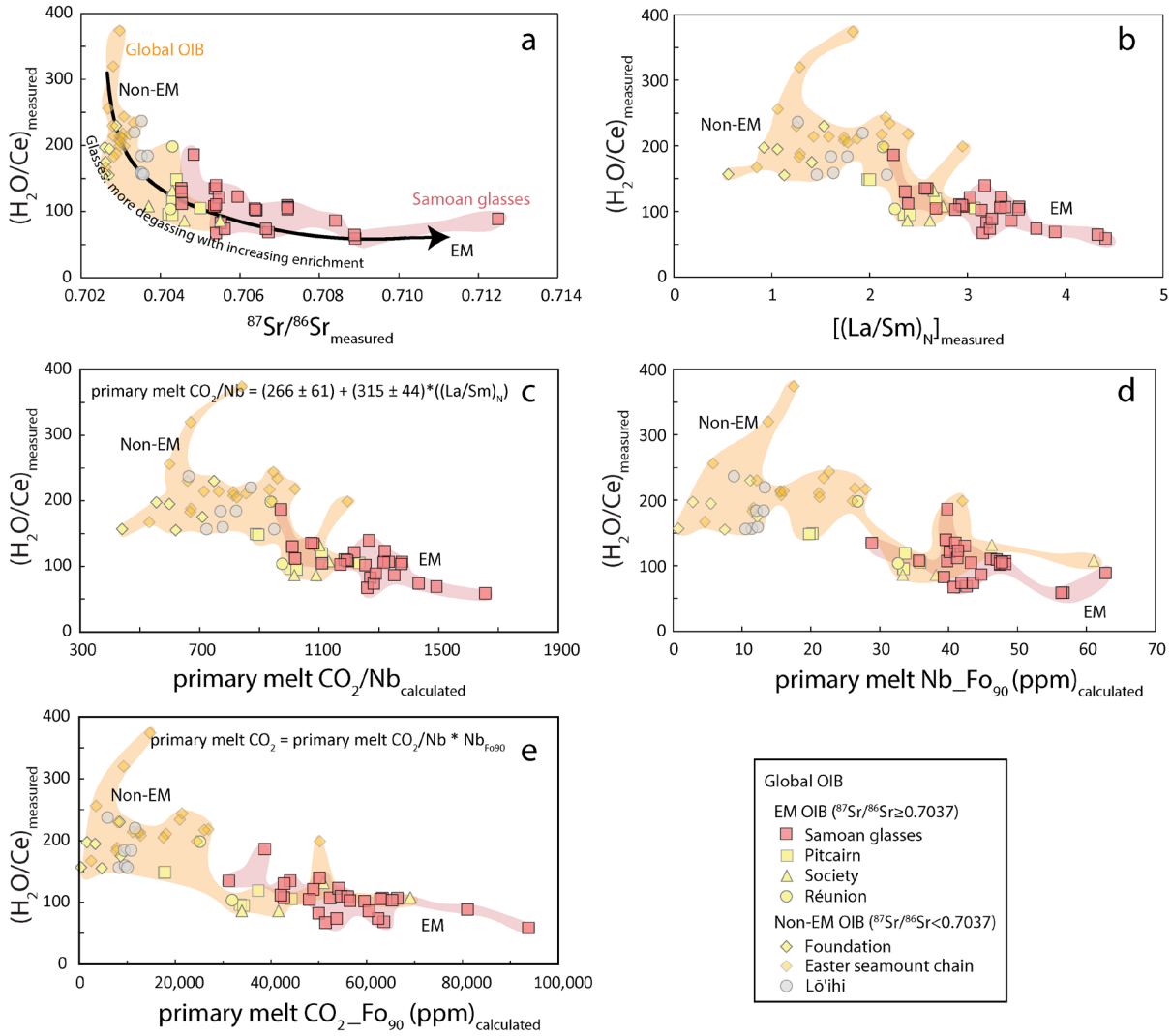

Figure 8. Samoan pillow glasses compared to a global dataset of submarine OIB glasses, which show a trend of decreasing H_2O/Ce with increasing $^{87}Sr/^{86}Sr$. The exact same OIB dataset is shown in all panels: only OIB with $^{87}Sr/^{86}Sr$ data (to establish the level of source enrichment) and MgO > 4.5 wt.% (to minimize the impact of fractional crystallization) are shown. (a) H_2O/Ce versus $^{87}Sr/^{86}Sr$. (b) H_2O/Ce versus $(La/Sm)_N$. (c) H_2O/Ce versus primary melt CO_2/Nb, where CO_2/Nb is calculated from the measured $(La/Sm)_N$ ratios using a linear fit between CO_2/Nb and $(La/Sm)_N$ (see equation shown in panel c) that is produced from a global data compilation of least degassed glasses and melt inclusions from OIB and MORB in Figure 9. (d) H_2O/Ce versus calculated primary melt Nb for each sample, where primary melt Nb is calculated by olivine addition (or subtraction) from melt—following methods in text—until the melt is in equilibrium with Fo_{90} olivine. (e) H_2O/Ce versus calculated primary melt CO_2, where the CO_2 is calculated for each lava by multiplying the calculated CO_2/Nb (panel c) with the calculated primary melt Nb (panel d) (see equation in panel e). The same sources of data and data treatment as that described in the Figure 7 caption are used here. The calculated primary melt CO_2/Nb and $CO_2\_Fo_{90}$ (ppm) values for the global OIB data set presented here are given in Table S11. Only samples with CO_2-H_2O saturation

1200 pressures ≥0.1 kbar are shown (just one Samoan glass with $^{87}Sr/^{86}Sr$ data has a saturation pressure <0.1
1201 kbar, sample AVON3-68-03 Rpt, so its removal does not significantly impact the dataset).

1202

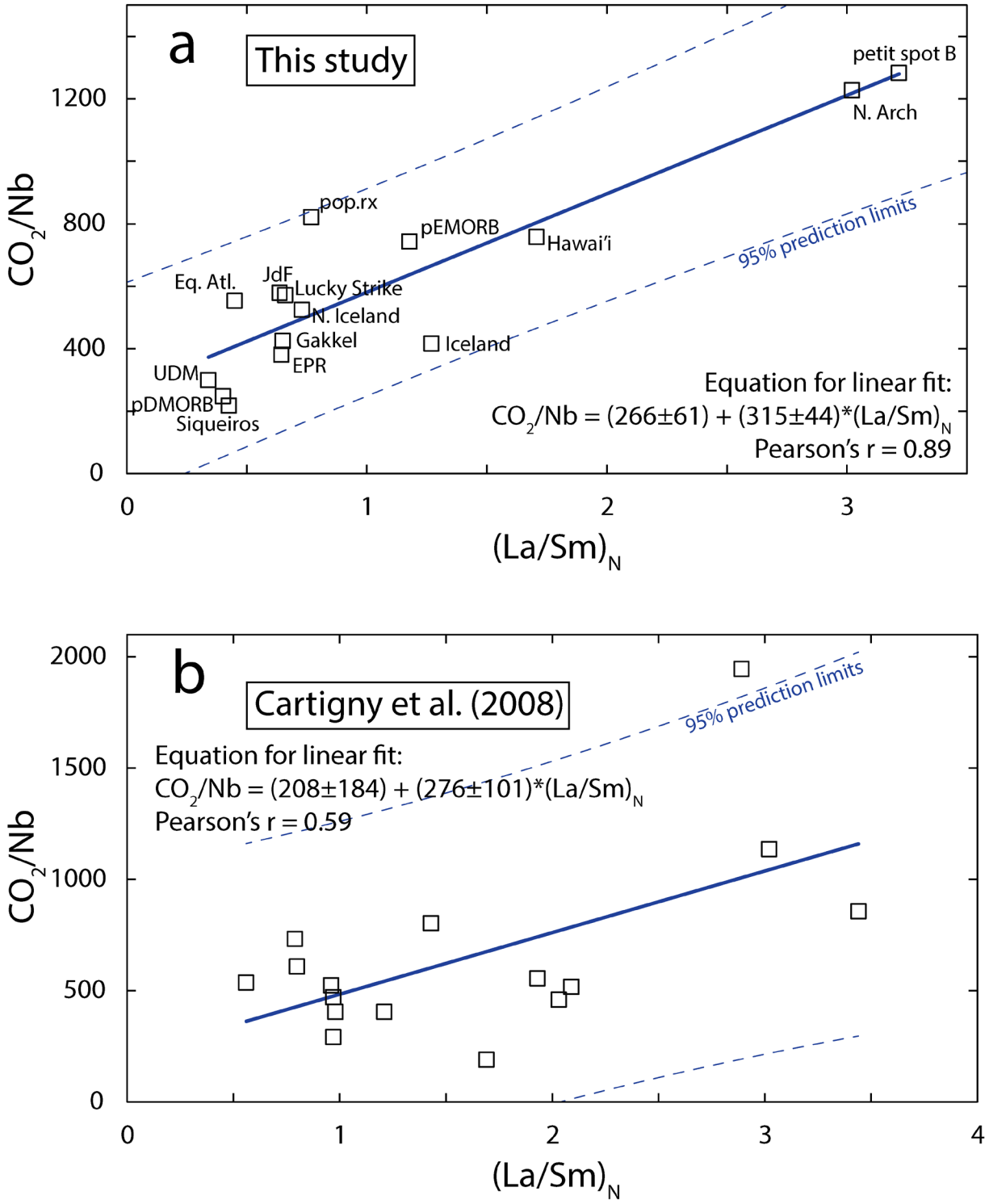

1203

Figure 9. (a) Linear fit (blue line) of global MORB and OIB glasses and melt inclusions with respect to CO_2/Nb and $(La/Sm)_N$. Data compilation is the same as what is presented in Figure 1 of Hirschmann (2018). The values for CO_2/Nb and $(La/Sm)_N$ in panel (a) are given in Table S10. The blue dashed lines represent the 95% prediction interval. The 95% confidence interval of the linear fit is given with the equation of the linear fit. The linear relationship calculated in panel a is used to estimate the CO_2/Nb values for glasses and melt inclusions in Figure 8. (b) Linear fit (blue line) to the Mid-Atlantic Ridge CO_2/Nb versus $(La/Sm)_N$ data from Cartigny et al. (2008). The blue dashed lines are the 95% prediction bands for the linear fit using Cartigny et al. (2008) data. Sources of data for panel a: L. Strike (Lucky Strike): Wanless et al. (2015); JdF, EPR (Juan de Fuca, East Pacific Rise): Wanless and Shaw (2012); Gakkel: Wanless et al. (2014); Siqueiros: Saal et al. (2002); pEMORB and pDMORB (Pacific enriched and depleted MORB): Shimizu et al. (2016); UDM (ultra-depleted MORB): Michael and Graham (2015); pop.rx (North Atlantic popping rocks): Cartigny et al. (2008); Eq. Atl. (Equatorial Atlantic): Le Voyer et al. (2017); Iceland: Hartley et al. (2014), Neave et al. (2014); N. Iceland (Borgarhraun): Hauri et al. (2018); N. Arch (North Arch, Hawai‘i): Dixon et al. (1997), Frey et al. (2000); Hawai‘i (Kīlauea): Anderson and Poland (2017); Petit Spot B (Western Pacific seamounts): Machida et al. (2015).

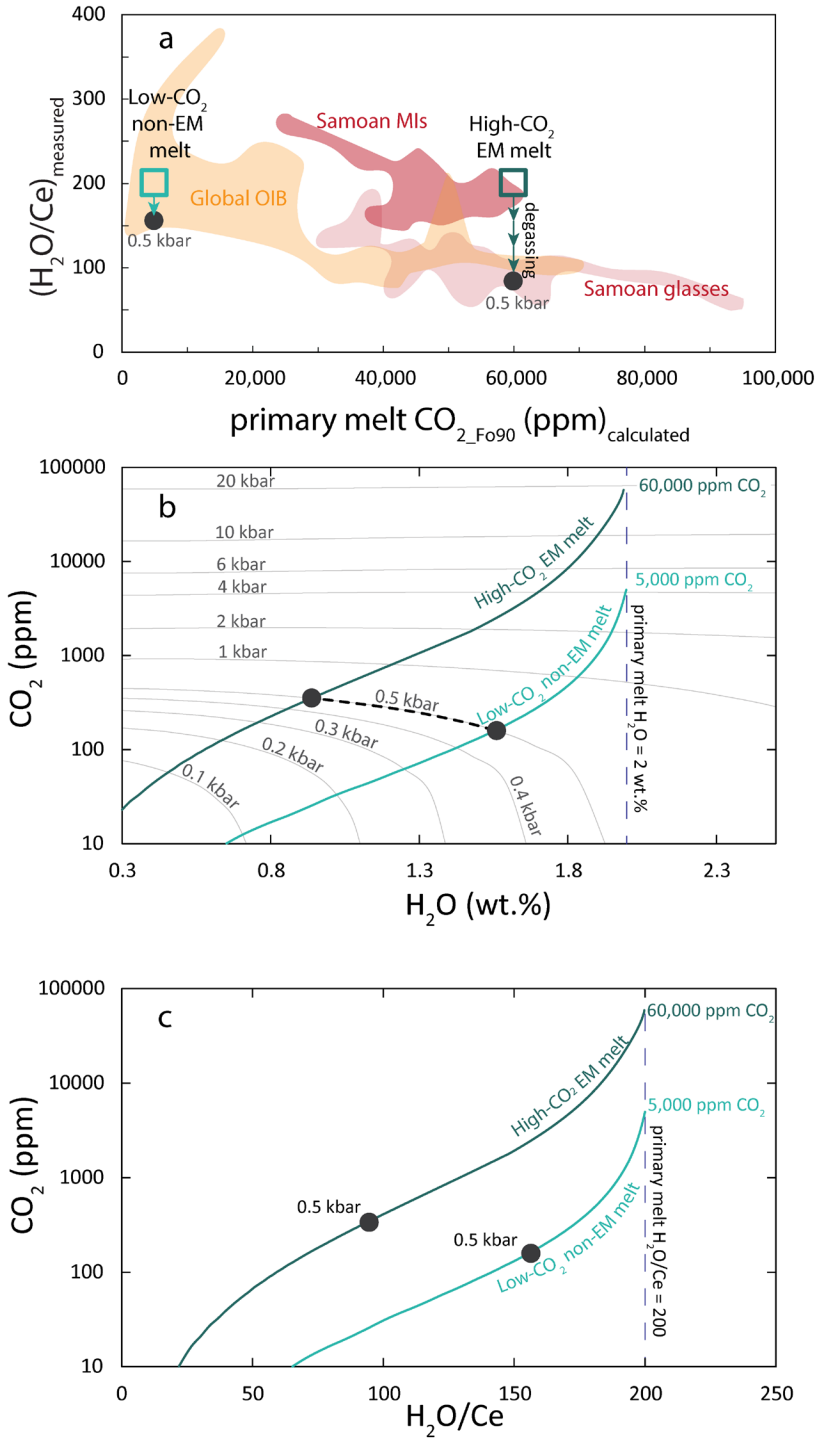

Figure 10. Figure illustrating how submarine glasses from enriched mantle (EM) sources acquire low H_2O/Ce relative to glasses from non-EM sources. We test two melt compositions that are identical in every way (major and trace element compositions are identical and H_2O is 2 wt.%) except for CO_2, where one melt starts with 60,000 ppm CO_2 (meant to represent an EM melt) and the other melt starts with 5000 ppm CO_2 (meant to represent the non-EM melt). (a) H_2O/Ce versus primary melt CO_2, reproduced in cartoon form from Figure 8e. The black circle indicates the H_2O/Ce value for melts at 0.5 kbar after

degassing. (b) In a plot of CO_2 versus H_2O, modeled closed system degassing paths show the impact of varying initial CO_2 on a melt that has the same initial H_2O content of 2 wt.%. While both melts start with the same initial H_2O, those with higher initial CO_2 degas more H_2O and have lower H_2O at a given isobar compared to a melt that has lower initial CO_2, demonstrating how higher initial CO_2 results in lower H_2O (and lower H_2O/Ce) in the erupted lavas. Degassing trends assume oxygen fugacity (QFM) and temperature (1200°C) and are calculated in rhyolite-MELTS v1.2 using AVON3-78-1#3 major element melt inclusion composition. Bottom panel shows the same degassing paths as the upper panels but shows H_2O/Ce instead of H_2O. Calculation of H_2O/Ce along the degassing paths assumes 1) an initial H_2O/Ce value of 200 (similar to the average H_2O/Ce value of Samoan melt inclusions examined here) and 2) a constant melt Ce concentration (100 ppm) that is calculated using the initial H_2O/Ce ratio (i.e., 200) and the initial H_2O (2 wt.%). Similar to the relationship between CO_2 and H_2O for high and low CO_2 melts, at a given isobar the melt with high initial CO_2 has significantly lower H_2O/Ce compared to the melt with lower initial CO_2. Isobars are calculated using MagmaSat for the average Malumalu melt inclusion composition at 1200°C. We consider only the case of M=0 to highlight the role of initial CO_2 and saturation pressure on the H_2O content of a glass, and non-zero M values would result in even more rapid H_2O loss.